Final Response to Anonymous Referee #1

We thank anonymous referee #1 for reviewing the manuscript and providing corrections and suggestions. Following are our point-by-point replies with the referee comments in italic. Page and line numbers refer to the marked-up revised manuscript, attached here after our replies.

General comments

The paper is well written and has an overall clear structure and figures. The topic is interesting and fits well to the aims and scopes of AMT. The authors identified two cloud features, bow and glory in the diurnal cycle of the cloud optical thickness and effective radius of stratocumulus clouds, which caused irregularities and could lead to misinterpretation by the user. The use of the two SEVIRI instruments onboard the Meteosat-8 and -10, which give the stereo perspective, is a great possibility to study these phenomena.

The sensitivity study focused only on the width of the droplet size distribution, which is important parameter and normally fixed for the cloud retrievals. The paper is valuable for people involved in cloud properties determination from image like SEVIRI measurements. The authors suggested two effective variance of the size distribution based on the sensitivity study. The whole study based only on two case studies. It is not shown that these two days are represented for a maritime and continual stratocumulus diurnal cycle, which should be included to make the results useful. Further the authors should discuss if this feature can be flagged for the user and include a suggestion how this cloud specific parameter could be used in standard retrievals as it mention in the abstract, but not discussed later.

It is true that in our study we did not examine the level of representativeness of the selected cases for typical conditions in the corresponding marine and continental clouds. In the revised manuscript we comment on similarities and differences in the diurnal evolution of the marine case with the study by Seethala et al. (2018), which evaluated the typical diurnal cycle of marine Sc clouds over the south Atlantic. Our case appears typical for the diurnal evolution of τ in this region, and less typical for r_e. However, in order to perform this analysis a near overcast cloud deck during a whole day relatively close to the equinox was needed, which is not easy to find.

The cloud bow and cloud glory features are related to retrievals falling outside the LUT, and these are already flagged, as we clarify in the revised manuscript (page 18, lines 3-5). Hence the users can already use this information to minimize their effects.

In principle the approach the authors present in their paper is very valuable and have great potential to understand cloud glory and cloud bow effects on the diurnal cycle of the cloud properties retrieved from satellite measurements. It is interesting and suitable for publication in AMT. However, I suggest the following revisions:

Abstract

Future climate data record is not mention or discussed in the paper at all, should be add in the discussion summary part.

The relevant part of Sect. 4 (last paragraph) was expanded with reference to the CLAAS-3 and CLARA-A3 plans to update the v_e value used, based on the findings of the present study. We also added more details on plans to attempt a retrieval of v_e based on the information available in the glory time slot.

Introduction

p. 3, line 4:

"Another issue in cloud optical properties retrieval, which relates to the cloud glory effects …" The citation from Mayer et al (2015) should come here already to motivate the sensitivity to ve. ("While under most retrieval circumstances the sensitivity of τ and re to ve is low, this is not the case for special illumination geometries, as was shown e.g. in Mayer et al. (2015) for the cloud glory conditions.")

This sentence was moved based on the referee's suggestion (page 3, lines 10-11).

p. 3, line 24.

This is inconsistent to the abstract the authors mentioned: " .. over different underlying surfaces (ocean/land) .." and here "..over the southeast Atlantic and one characteristic day"

We clarified this part by mentioning both the studied regions (page 3, lines 29-30).

p.3 line 26-28.

Should be move to the summary: " While … properties."

This sentence was moved to the beginning of Section 4.

Data and Methodology

p.6 line 4-7. "It relies on … illumination conditions." This have not to repeat again. I would suggest to shorten this part. (see p.2 line 22-27.)

The same piece of information was indeed repeated. We have shortened this part (page 6, lines 17-19).

p. 8 line 2. Why only two days? Please discuss.

Cloud glory and bow, and the ensuing irregularities in the retrievals, occur in specific time slots depending on the region. In order to combine both features in the analysis, we needed to narrow our selection of days to cases close to an equinox, when cloud glory features manifest. Hence, their study was necessarily limited to small areas and specific days. We have added this information in page 3, lines 26-29 of the revised manuscript. Irregularities due to cloud bow and glory conditions in the diurnal evolution of clouds will occur no matter how that diurnal cycle exactly looks. Hence, the diurnal evolution in the selected day(s) does not have to be representative of the specific cloud types and regions. In cases with variable cloudiness during the day, the impact of the cloud bow and glory features on the cloud property diurnal cycle may be blurred. Therefore, we searched for near-ideal cases in terms of cloud cover in a sufficiently large region during the full day.

It would be useful to have RGB images for the two days and two satellite on a time slot.

Compared to similar studies (e.g. Cho et al. (2015)), the areas under study are rather small (2°×2° based on the revised analysis) and covered to a large extent (more than 80%) by clouds. Hence we think that an RGB image would not add useful information, also considering that the analysis was mainly based on spatial averages.

Results

For the spatially averaged reflectances it would be interesting to see the variation (max and min cloud glory and cloud bow effects) and the propagation to the CPP algorithm.

Cloud bow and glory conditions lead to a momentary increase in reflectances in both the visible and the SWIR channels. This is depicted in Figs. 4c and 4e for the spatial averages, but it is true overall on a pixel basis. The histogram below shows an example of changes in reflectance at 1.6 μm from MSG-1, on 7/3/2017 over the southeastern Atlantic region, from 08:30 UTC, which is a "normal" time slot, to 08:45 UTC, which is affected by glory (see also Fig. 4e).

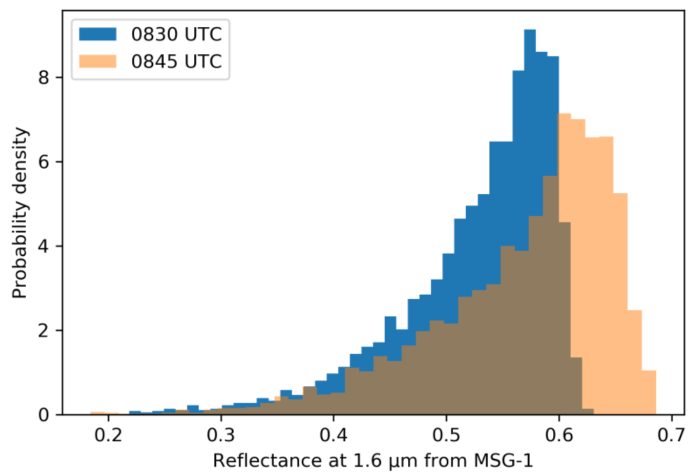

Propagation of this temporary "jump" to the CPP output is not straightforward to visualize, since the LUT, from which the output is retrieved, also changes shape through time. These changes ideally will compensate for the "jumps" in reflectances and lead to a diurnally smooth output. In practice, twists and folds in the LUTs (see e.g. Fig. 5a) lead pixels with extreme reflectance values to fall outside the LUT. These pixels are flagged, but retrievals are still performed, giving extreme output values. The retrieved r_e values corresponding to the histograms above are shown below.

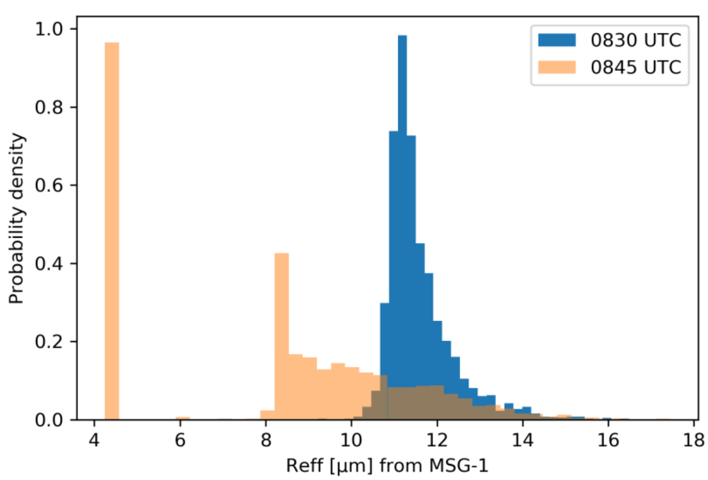

Obviously in this case the glory causes many pixels to lie above the LUT, leading to an unnatural peak in low r_e values. These extreme retrievals lead to jumps when included in the spatial averages (see also Fig. 4f). A user should of course avoid using these flagged pixels. In our study, however, the aim is to analyze these cases and their effects, so their inclusion in the analysis was self-evident.

Figure 4: The dotted and dashed line are hard to distinguish. For example, dotted dashed line and dotted line, should be better.

We have added letters next to each vertical line, denoting either cloud bow (b) or glory (g).

p. 14, line 13. Expression "more natural output" , please rephrase.

This expression was rephrased (page 18, lines 2-3).

p. 15, line 8. "this does not necessarily mean that the actual droplet size distribution is so narrow." Should be discussed how this could be verified in the conclusion.

The purpose of this sentence was to state that the smoothness of the diurnal curve around the glory is not directly linked to the retrieval failures depicted in Fig. 9. However, this is not directly supported by the analysis, and it was removed from the revised version.

Discussion and Summary

The authors should more discuss if this feature can be flagged for the user and include a suggestion how this cloud specific parameter could be used in standard retrievals as it mention in the abstract.

The irregularities in cloud bow and cloud glory can already be avoided to some extent by the user, since they are associated with pixels falling outside the retrieval LUT, and these pixels are flagged (see also Fig. 9 and relevant discussion). Based on our findings, an updated value of v_e will also be used in future retrievals of CLAAS and CLARA. This information was included in the last paragraph of the revised Sect. 4.

p. 19, line 12. How often do these irregularities happen?

Based on the way scattering angles change during a day, cloud bow irregularities will manifest twice per day in any region. Irregularities associated with cloud glory require high values of scattering angles. Due to the position of both satellites along the equator, these conditions are met in days close to the two equinoxes. This information was added in the revision (page 24, lines 16-18 and page 25, line 1).

Should be critical discussed that the finding depends on the optical thickness of the cloud and the cloud types.

The effect of τ on the cloud bow irregularities was already discussed in Sect. 3.4 (page 21, line 27 and page 22, lines 1-2). On the other hand, cloud glory irregularities on τ appear in both low and high τ cases.

Typo

p.4 line 9: Data and Methodology

Corrected.

Final Response to Anonymous Referee #2

We thank anonymous referee #2 for reviewing the manuscript and providing corrections and suggestions. Following are our point-by-point replies with the referee comments in italic. Page and line numbers refer to the marked-up revised manuscript, attached here after our replies.

Figures 6 and 11 show phase functions at intervals of angles of cloud bow and glory. It is seen that the phase functions are very sensitive to the effective size and to the effective variance. The reflectance of a cloud as measured from satellite at the top-of-atmosphere should be less sensitive because of multiple scattering. It would be instructive to provide figures of angular dependence of the reflectance as additional figures along with Figs 6 and 11. Additional figures can be done for one typical value of the cloud optical thickness, say 8, using the LUTs created by the authors. One observation geometry, say MSG-3 and the region west of the African coast, will be enough. Some of the Sun-satellite geometry angles can be constant and correspond to the case of March 7, 2017. The geometry angles should vary so that the intervals of scattering angles correspond to the intervals angles of Figs 6 and 11.

The analysis proposed by the reviewer was included in our results (page 14, lines 2-12). We have selected the southeastern Atlantic region and the MSG-1 observation geometry, whereby both cloud bow and glory effects are apparent in the reflectances (Figs. 4c and 4e), during the same day (March 7, 2017). For each time slot, the viewing and illumination geometry and the effective radius were those calculated from the spatial averages of the actual retrievals, while three values of cloud optical thickness were examined: τ = 1 (very thin cloud), τ = 8 (close to the average retrieved value) and τ = 30 (thick cloud). Using the LUT with v_e = 0.15, we plotted the reflectances in the 0.6 µm channel corresponding to these cases. The results clearly show how an increased τ increases the reflectance measured by the satellite sensor. They also confirm that the cloud glory and cloud bow reflectance magnitudes relative to non-glory and non-bow time slots are not affected by τ, which was already mentioned in the manuscript for the cloud bow case. As Mayer et al. (2004) nicely described it: “The glory structure sits on top of a multiple-scattering background which of course depends on optical thickness”.

Figures 12 and 13 show retrievals results for 0.6 µm - 1.6 µm channels and 0.6 µm - 3.9 µm channels separately. There is difference in the retrieved values, especially for the effective size. Sensitivity to the effective variance is seen as well. The authors should discuss how those properties can be used to estimate the effective variance.

Possible ways to estimate the effective variance are discussed in the last paragraph of Sect. 4 in the revised manuscript. They are not based, however, on the differences in retrievals using the two different spectral pairs, as the reviewer suggests. As we discuss in the marine case, where these differences are also present, they should be attributed to the different penetration depth of the 1.6 µm and the 3.9 µm wavelengths (page 19, lines 12-14), and possible shortcomings in the treatment of the 3.9 µm channel (page 21, lines 11-12).

Technical corrections.

Page 3 line 16 Replace Mayer et al. (2015) by Mayer et al. (2004).

Done.

The dotted and dashed lines are hardly distinguished in figures. I would prefer to see straight vertical lines of different color.

We have added letters next to each vertical line, denoting either cloud bow (b) or glory (g).

Final Response to Anonymous Referee #3

We thank anonymous referee #3 for reviewing the manuscript and providing corrections and suggestions. Following are our point-by-point replies with the referee comments in italic. Page and line numbers refer to the marked-up revised manuscript, attached here after our replies.

Specific comments

The paper combines methodologies mainly from Arduini et al. (2005) and Cho et al. (2015) with the results of Mayer et al. (2004).

The main deficiencies of the paper:

1. The authors talk about the cloudbow effect for scattering angles close to 140° (page 2, line 32) and the "collapse" of the phase function at a scattering angle of 132° and cite to this end the results of Cho et al. (2015) about retrieval failures for MODIS. Similarly, they cite this paper for the glory effect that also leads to retrieval failures for MODIS, but they also mention the work by Mayer et al. (2004) that uses the feature of the liquid cloud phase function around the backscatter direction to retrieve optical thickness, effective radius and effective variance of the particle size distribution. I think that in this paper two different effects are mixed together: on one side, the "bumps" in the phase function observed at the bow and glory geometries; on the other side the reduced sensitivity of the observations to effective radius due to the "collapse" of the phase function close to the same observation geometries.
An increased phase function intensity for particular scattering angles has as a consequence "stripes" of higher reflectivity for these scattering angles (as observed by Mayer et al. (2004) in the glory region) that, on their turn, could have as a consequence artificial "stripes" of higher optical thickness when the underlying LUT in the Nakajima-King retrievals does not consider these features (e.g. because of an unsufficient angular sampling of the phase function).
The "collapse" of the phase function instead produces retrieval failures due to the fact that the LUTs are narrower, especially for thin clouds, such that the retrieval is more prone to failure because the retrieval/radiative transfer/calibration uncertainties can "push" the observation out of the LUT more easily (cited more or less literally from Cho et al. (2015)). However, this collapse takes place in this paper (Fig. 5) at 132° and is *the cloudbow effect found in Cho et al. (2015). The authors explain this effect in a nice way, but they assert that "in the cloud bow time slots retrievals are rather normal, with big differences occurring in r_e for smaller scattering angles, namely close to 132°" (page 10, line 15-16). Thus, they mix up these two aspects that shall be separated clearly in the revised version of the manuscript. Correspondingly, it shall also be considered to plot the "collapse" angles instead of the cloudbow angles.*

It is true that the cloud bow and glory, on one hand, and the collapse of the phase functions, on the other, are two different effects, which we did not intend to mix. These effects are examined together in this study because they both cause irregularities in the retrievals. However, we think that mentioning that the effects of "collapse" occur "near" the cloud bow or glory, which we already mention in the first manuscript version (page 3, line 20), helps making their description simpler. In the revised manuscript, we try to clarify this further (page 3, lines 1).

While we have verified that our LUTs adequately consider the increased phase function intensity for these features, at least regarding the angular sampling, we also show that this phase function intensity is highly sensitive to the value of the effective variance (Fig. 6b), which has to be assumed. This sensitivity can explain the corresponding differences reported in cloud optical thickness for time slots around glory conditions, as we show e.g. in Figs. 7 and 8.

The problem caused by the collapse of the phase functions is indeed different, but it occurs *close to* the cloud bow, which is a "bump" in the phase function, as the reviewer describes. Hence, we don't understand why the statement in page 10, lines 15-16 of the initial manuscript is problematic. We think that it clearly separates the cases of cloud bow from those of scattering angles where the "collapse" occurs. Although Cho et al. (2015) describe similar failures as a "cloud bow effect", they clearly show their relation to the scattering angles where the phase functions collapse, and not to the local maximum in the phase function intensity, which defines the cloud bow. Both in the initial and the revised manuscript, we try to be specific regarding this discrimination, and a similar one regarding the cloud glory (see also our next reply), by using regularly the terms "near the cloud bow" and "around the cloud glory". However, starting the analysis with the observed reflectances, (Fig. 4c and e), we opted to plot the cloud bow angles, where reflectances peak locally.

As far as the glory is concerned, I would suggest not to talk about maximum scattering angles and label them as "glory" (page 18, line 6) but to check the behavior of the phase function for angles larger than say 170° and then argument whether a particular effect on the cloud retrieval is expected at all (and in case which effect) or not. In this sense I think that also the information about the 0.6 μm phase function used in the argumentation on page 18, line 5-10 should be shown. Furthermore, the same effect in this scattering angle range (glory) might be expected as for the cloudbow as is explained in Cho et al. (2015). The "collapse" of the phase function mentioned at 132° is the most clear one, but Cho et al. (2015) identify further angles where this reduced sensitivity is also observed: they find 133°, 142° and 177° for their MODIS example. Even if at slightly different angles, this effect is present in this manuscript as well (see Fig. 5c and Fig. 6a) and could be the reason for the irregularities investigated. In particular, the 177° angle is a "glory angle" such that retrieval failures in this scattering angle range might also be traced back to a "phase function collapse".
These aspects shall be addressed in more clarity and the analysis adapted.

It is true that the "maximum scattering angles" do not always coincide with a local maximum in the phase function intensity, which defines glory conditions, and this part was corrected accordingly. Nevertheless, the difference in scattering angles between adjacent 15-min time slots is of the order of 3°, ensuring that glory conditions will occur (perhaps more than once) close to this maximum. This probably explains also the difference in the shape of irregularities around the glory between MSG-1 and MSG-3 (see e.g. Fig. 8). Plotting the maximum scattering angles was rather selected as a common reference to guide the eye to the "center" of the period when glory effects occur. We clarify this point in page 11, lines 10-12 of the revised manuscript.

The referee's suggestion, namely to first check the behavior of the phase function for large angles and then argue whether a particular effect should be expected, is not feasible in our case, since it would imply that we already know the exact shape of the phase function, which depends on the effective variance.

Information about the 0.6 μm phase function is now included in Fig. 6b.

Following the referee's suggestion, in the revised manuscript we repeat the approach followed by Cho et al. (2015) and calculate separation indices for every group of phase functions we examine, in terms of both different r_e values and different v_e values (page 13, lines 20-30). This is a nice way to visualize and quantify the effect of "collapsing" phase functions on the retrieval process and helps in the interpretation of corresponding results. Our results verify the presence of "collapsing" conditions in the abovementioned scattering angles. It should be pointed out, however, that the 177° is not always a “glory angle”, since it depends on the wavelength examined.

2. To observe the effects described above I find the approach of using two fixed regions where the results of τ and r_e are averaged (I think at least they are averaged: page 9 line 3-4 is not completely clear in this respect) to be not optimal since it might wash out the effects. In fact, all these “ripples” in the phase function take place in few degrees such that the approach of using regions with 5°×5° or 4°×4° size may complicate the identification and explanation of the related retrieval effects. In this sense, do for instance all pixels at 9 UTC in Fig. 4 have maximum scattering angle? I think that it should be discussed how strong the scattering angle can vary inside a SEVIRI pixel and inside the regions investigated in order to assess whether the expected effects can be identified or to what extent they are weakened by the averaging procedure. Furthermore, for a clearer illustration of the results I think that an additional picture showing one area (i.e. a 2D plot in latitude and longitude) in the cloudbow and/or glory slot would help interpreting the results (similarly to Fig. 10 in Cho et al. (2015)).

The results in Fig. 4 are averaged, as are the reflectances. We clarify this point in page 10, lines 11-13 of the revised manuscript. The range of scattering angle values for each satellite and time slot was also quantified. Typical ranges for the southern Atlantic region are 0.91°±0.11° and 1.01°±0.11° for MSG-1 and MSG-3, respectively. It was also verified that the maximum scattering angle occurs in the same time slot for every pixel in both MSG-1 and MSG-3. While these results ensure no complication due to the size of the areas selected or the 15-min frequency of observations, we also examined averaging in smaller areas, based on the reviewer’s concerns. We found that using 2°×2° areas we could still identify the effects under study, without increasing significantly the variability between time slots, which could compromise our results. However, the area covered with liquid clouds was significantly increased (Fig. 3 of the revised manuscript), and typical variations of scattering angle values within a time slot dropped to about 0.4°, providing a better correspondence between averaged retrievals and phase function characteristics. This is highlighted in page 11, lines 11-13 and page 12, lines 1-2 of the revised manuscript. Hence, we decided to repeat the analysis based on this reduced (2°×2°) area size.

However, the study areas are much smaller compared to the area shown in Fig. 10 of Cho et al. (2015) (~20°×20°), and uniformly covered with liquid clouds. Hence, adding a picture showing one of the areas would not provide any additional help in the interpretation of the results.

3. Fig. 6b shows that there are angles of reduced sensitivity to the effective variance while most of the phase function shows a clear dependence on v_e in this angle range. Can you see this “collapse” of the phase function w.r.t. v_e in Fig. 7? Does this dependency of the phase function on v_e extend to other scattering angles as well? Looking at Fig. 2 it would be interesting to shortly explain where an effect due to the dependence of the phase function on v_e can be expected.

A collapse of the phase function with respect to r_e, shown e.g. in Figs. 5c and 6a, leads to an irregularity in the r_e retrieval (e.g. Figs. 8c and 8d near the cloud bow angle), independently of the v_e value, which is selected *a priori*. This happens because phase functions collapse close to the cloud bow angular region no matter the v_e value selected. Correspondingly, we should expect a reduced sensitivity in an attempt to retrieve v_e in angles where phase functions of Fig. 6b collapse. Hence, the effect of the collapses in Fig. 6b cannot be seen in the results of Fig. 7. The irregularities in the r_e retrieval around the maximum scattering angles (Figs. 7b, 8c and 8d), occurring especially for larger v_e values, are rather associated with increased “collapsing” of the phase functions in the backscattering region for larger v_e values, which leads to higher separation index values and hence more points falling outside the LUT.

4. It has never been clearly stated in the manuscript whether the "flagged pixels" (e.g. page 14, line 14) contribute to the plots (e.g. Fig. 4). However, page 10 line 24-25 suggests that the τ - r_e results for the flagged pixels are used for the statistics (i.e. the diurnal cycles). From my point of view, these flagged pixels correspond to the failures investigated in Cho et al. (2015) and thus should not be used.
Similarly, do you show in Fig. 4c,4e the mean reflectance of the box or the mean cloud reflectance? This uncertainty arises from the phrasing "used as input to the CPP algorithm" (page 9, line 2) which seems to imply that you mean the cloudy pixels alone, since no retrieval is run for cloudfree pixels, I suppose. And what about the scattering angles/optical thickness/effective radius?

"Flagged pixels", i.e. those falling outside the LUT, are indeed used in the diurnal plots. The purpose of providing flags in a data record is of course to inform the user on possible failures and reliability issues, and in that sense we agree with the reviewer that they should be excluded from a study using these data. In the present study, however, our purpose is to highlight the irregularities caused by these failures, and investigate their origin and ways to reduce their effects. Furthermore, exclusion of these pixels would cause gaps in the diurnal variation, or at least not directly comparable adjacent time slots, since flagged pixels cover large parts of the study areas in the specific time slots studied (Fig. 9).

The mean reflectance in Figs. 4c and 4e are mean liquid cloud reflectance, to be directly comparable with the CPP retrievals, which are also averaged over liquid clouds only. Scattering angles are averaged over the entire area. The almost complete coverage of the study areas with liquid clouds ensures that possible discrepancies are minimized. This is especially true for the revised results (see also revised Fig. 3). All these points are clarified in the revised manuscript (page 10, lines 11-13 and page 10, lines 15-16).

5. In Fig. 4, the cloud glory regions (red and black) show different behaviours: the red one (MSG-1) shows a strong irregularity made up of two strong local minima and one local maximum in the optical thickness plot (d), while the black one (MSG-3) shows a weak local mimimum alone. Please explain why there is this difference.

This difference should be attributed to the different scattering angles from the two satellites. The small differences, combined with the high sensitivity of the scattering phase functions in the backscattering directions, led to these different behaviors.

6. I am missing an overall discussion about the plausibility of the retrieved diurnal cycles. This would increase also the plausibility of the investigations shown in the entire paper. For instance:

- *Can one expect that marine Sc has an almost flat re diurnal cycle (Fig. 4) while the optical thickness is decreasing strongly, a hint that the thermodynamic conditions the clouds are developing in are changing during the course of the day?*

  It is true that the flat r_e diurnal cycle, combined with the strongly decreasing τ, is not the average behavior of the marine Sc, where a decrease in r_e would typically be expected (see e.g. Seethala et al., 2018). However, this is an one-day case, hence not necessarily representative of the average. We discuss this point in page 10, lines 14-15 of the revised manuscript.

- *The diurnal cycles in Fig. 4 and Fig. 10 differ: the 3.9 μm retrieval produces a lower τ and a lower r_e, although in an adiabatic environment one would expect higher r_e at the cloud top, where the 3.9 μm retrieval is more sensitive. If you think that "subpixels fractions of open water" (page 17 line 9-10) are the reason for this, you might take a look at the HRV channel, if it is available over* *these regions, for a first check about this hypothesis. What is the uncertainty of the 3.9 µm retrieval, which should be higher than the one for the 1.6 µm?*

The study area is very homogeneously covered with clouds (and even more so is the adjusted 2°×2° area), and therefore the presence of subpixel fractions of open water is highly unlikely. We believe that potential imperfections in the treatment of the 3.9 µm channel (e.g., calibration, atmospheric absorption) are the most likely explanation for the differences between the 1.6 µm and 3.9 µm retrievals.

The calculated uncertainty in the 3.9 µm retrievals is overall somewhat lower than in the 1.6 µm retrieval. The probable explanation for this is that presently no uncertainty due to atmospheric absorption and the thermal contribution in the 3.9 µm retrievals is included in the calculations.

- *MSG-1 and MSG-3 in Fig. 10 provide different diurnal cycles of r_e. While MSG-1 seems to observe a decrease in re at around 9 UTC, MSG-3 yields an increase and a decrease afterwards.*

  The decrease in r_e retrieved from MSG-1 at around 9 UTC, also apparent based on the new results, is due to the glory conditions affecting the retrieval. Examining non-affected time slots, it can be seen that MSG-1 and MSG-3 retrievals are quite similar, with increasing r_e before 9 UTC and slightly decreasing after 10 UTC.

- *In Fig. 12 MSG-1 and MSG-3 also provide very different diurnal cycles: not only the absolute values but also the variations in time are different, both in τ as well as in r_e. How can this be explained? Such strong differences preclude of course the use of simultaneous observations of the two satellites, both for physical/meteorological investigations of cloud properties and for the purpose of the present paper.*

  It is true that there are many differences between MSG-1 and MSG-3 retrievals over the continental region, based also on the smaller study area of the revised manuscript. Although we are not certain on the reasons behind these differences, they are probably related to specific cloud types and 3D effects, since no similar issues were found in the marine case. These differences were not investigated further, since they don't actually preclude the separate use of the two sensors for the purpose of the present study: the simultaneous usage of the two satellites, which was based on the assumption that retrievals are the same, was dropped earlier in the study for practical reasons (see page 15, lines 9-10). The differences between MSG-1 and MSG-3 should indeed be of high concern if the previous assumption was required, and we highlight this point on page 15, lines 10-11 of the revised manuscript. In Section 3.4, however, they are only analyzed in parallel, to highlight the same effects based on different illumination and viewing conditions. However, since this point is important, we also included a small discussion acknowledging this issue (page 22, lines 12-16).

7. The continental case is said to be "not directly comparable with the marine Sc case" (page 18, line 5). If this case is shown, and I think the paper benefits from this since it shows a cloud with higher optical thickness and much higher effective radius, it should be done in more detail: see my comment above about the phase function and the explanation of the diurnal cycles. Further aspects that are not completely clear for this case are the fact that τ shows a dependency on v_e while r_e shows none in the glory geometry, and the short temporal displacement between the small local minima in τ for the cloudbow and the local maxima in r_e (Fig. 12).

Section 3.4 was expanded in the revised manuscript based on the aspects raised by the reviewer, as well as on the additional analyses of uncertainties and separation indices. Our arguments regarding differences between τ and r_e under glory conditions were based primarily on the characteristics of the 0.6 µm and 1.6 µm phase functions.

8. Retrieval results still seem to show a relatively small variability w.r.t. v_e. Is this sensitivity to v_e comparable to the retrieval uncertainties or retrieval errors or is it larger?

While it is not clear to which retrieval results the reviewer refers to, it is indeed crucial for the validity of our conclusions to compare the variability w.r.t v_e with retrieval uncertainties. For this reason we used the methodology described in Stengel et al. (2017) to propagate the level 2 retrieval uncertainties to the spatially averaged values used in this study. We describe the process used in page 8, lines 8-14 and page 9, lines 1-2. In the Results section of the revised manuscript, it is also explicitly mentioned if the v_e variability is smaller or larger than the propagated uncertainty.

9. The manuscript demonstrates that particular geometries like the cloudbow and the glory can lead to biased optical properties, but what would you propose in order to reduce this bias, keeping in mind that in 15 minutes (from one slot to the next) also cloud physics can vary (the cloud can thin out, become thicker, its particle size distribution can change...)?

Based on our results, we propose that using more appropriate values of effective variance can help reducing the biases associated with the cloud glory geometry (page 26, lines 13-14). While cloud properties indeed vary within 15 minutes, this variability is not apparent in our spatially averaged analysis. On a pixel basis, this variability is expected to be more pronounced, but correcting the size distribution as we propose would still remove the additional irregularities.

10. The paper should shortly discuss/mention at one place the reasons why the same retrieval from two satellites at the different locations could yield different results, apart because of glory and cloudbow. Here I think of shadow effects, partially cloudy pixels, cloud inhomogeneities, 3D radiation effects, surface BRDF, mixed phase clouds, misidentification of thin cirrus on top... This is the basis for the synergistic use of the two MSG spacecraft. Parts of this discussion are e.g. at page 8 line 8 and page 10 line 11.

This is indeed an important part of the discussion that we included in page 4, lines 11-18.

Further comments:

***Title**: Since the paper presents results for two selected days over two selected regions I recommend to add "A case study" somewhere to the title.*

While the paper indeed examines two selected days, we would hesitate to characterize it as a "case study" for two main reasons: (a) any further averaging of data, either in space or in time, would render the cloud bow and glory phenomena impossible to study, since their effects are restricted in both space and time. Hence, this study cannot be conducted on a "bulk-data" basis. (b) The notion of "case study" usually refers to a phenomenon of particular interest, which manifests as a specific event (e.g. extreme weather event). However, the days studied here were chosen based only on specific criteria that were met. The phenomena studied occur around the globe on a daily basis.

Abstract: *Please mention that you analysed two days of data.*

Done.

Figures:

• I suggest to merge Fig. 3a with Fig. 4 and Fig. 3b with Fig. 12.

We opted to keep the figures separated, because we wanted to highlight from the beginning that both study regions met (and were selected based on) the high coverage with liquid clouds criterion. Furthermore, Fig. 4 would become too “busy” with such a merging.

• Please use the same colors for MSG-1 and MSG-3 in all figures.

The reviewer probably refers to Fig. 3, where colors were swapped. This is now corrected.

• Please add the solar zenith angle to Fig. 4 in order to understand when θ_0 is reaching 90°, i.e. sunrise and sunset. This might explain for instance the increasing reflectance at 0.6 µm in Fig. 4c and 4e.

The solar zenith angle in these plots is always less than 84.3°. In fact, this is the threshold for CPP retrievals used in CLAAS-2 and applied throughout this study. This is mentioned in Table 1 but is further clarified in the revision (page 9, lines 20-21). Hence, sunrise and sunset cannot explain the increasing reflectances in Figs. 4c and 4e, and adding the solar zenith angle to Fig. 4 would not be useful. As explained in a later comment (page 10 of this document), the increasing reflectances are probably due to the high solar zenith angle combined with the higher viewing angle from MSG-1 compared to MSG-3. This difference in reflectance, however, is not repeated in the CPP output, showing that these conditions are accounted for in the retrieval.

• I suggest to move Fig. 5c to Fig. 6.

Figure 5c was placed next to the LUT diagrams of Figs. 5a and 5b to highlight the effect of the “collapse” of the phase functions at 132° on the corresponding LUT depicted in Fig. 5a. The phase functions of Fig. 6 focus on the backscattering directions and the relevant discussion refers to cloud glory. For this reason we think that it is better to keep Fig. 5c and Fig. 6 separated.

• For all figures with glory and cloudbow: it would be helpful for the reader to write directly into the plot which vertical line is glory and which one is cloudbow.

We have added letters next to each vertical line, denoting either cloud bow (b) or glory (g).

• For all figures with diurnal cycles: it would be easier for the reader if each panel contained MSG-1 or MSG-3 somewhere to distinguish the satellites at a glance.

Done.

• Since only hours are used in the diurnal cycle plots I think that e.g. “05” or “5” would be better than “0500”.

Done.

• Units should be expresses either as e.g. “Θ / degree” or “Θ [degree]” but not “Θ (degree)”. Furthermore “Reflectance (0.6 μm)” should read “Reflectance at 0.6 μm” with no unit. Instead of “Hour (UTC)” I suggest “UTC hour”.

Done.

• Fig. 5 is too small. Furthermore, it is probably not a “scatter plot” (page 10, line 25-26) but I guess a 2D histogram. In that case the colors should be explained as well.

Indeed, the term “density plot” explains better what Figs. 5a and 5b show (page 13, lines 3). The colors are also explained in the revised figure caption.

• Please add a (dotted) line at height 0 (r_e or τ difference = 0) in Fig. 7.

Done.

***Page 4, line 21**: I cannot believe that the MSG-1 satellite is moving so fast and so much (10° latitude in 24 h) around its subsatellite point. Please check this in more detail! This could have an important impact of the observation geometry.*

Sub-satellite point coordinates are available in the original MSG SEVIRI files metadata, while EUMETSAT has also warned users on this issue (see e.g. www.eumetsat.int/website/home/News/ConferencesandEvents/DAT_3647214.html). This deviation, however, should not be seen as an independent movement of the satellite around the nominal sub-satellite point, but rather as the satellite lying in an orbital plane inclined by about 5° compared to the equatorial plane. While the impact on the observation geometry can indeed be important, inclusion of this information in our retrievals actually ensures avoidance of possible misinterpretations.

***Page 6, line 21**: Why do you need three values of the surface albedo?*

The explanation for this is somewhat technical. The cloud reflectance can be written as the sum of the reflectance for a dark underlying surface and a term containing cloud transmittance, the hemispherical sky albedo for upwelling isotropic radiation, and the actual surface albedo. From radiative transfer simulations of the cloud reflectance at two particular surface albedos (chosen as 0.5 and 1 for numerical stability), the transmittance (function of zenith angle) and sky albedo can be determined. These are also stored in the look-up table and then allow the direct calculation of cloud reflectance for any value of the surface albedo. This procedure is described in the CM SAF CLAAS-2 ATBD, and a reference to this ATBD has been added in the manuscript (CM SAF, 2016a; page 7, lines 12).

***Page 6, line 24-27**: Please give a reference (or a short explanation) for the gas absorption correction and the thermal emission consideration.*

The gas absorption correction method is explained in the CM SAF CLAAS-2 ATBD. The thermal emission calculation is not covered by the CLAAS-2 ATBD because CLAAS-2 does not involve the 3.9 μm channel. However, the CPP algorithm has also been applied to AVHRR for the production of the CLARA-A2 data record. In that context, the AVHRR 3.7 μm channel is used, and the consideration of thermal emission is covered in the corresponding ATBD, which has been added to the main text (page 7, line 10) and the reference list:

CM SAF: Algorithm Theoretical Basis Document, CM SAF Cloud, Albedo, Radiation data record, AVHRR-based, Edition 2 (CLARA-A2), Cloud Physical Products, EUMETSAT Satellite Application Facility on Climate Monitoring, SAF/CM/SMHI/ATBD/CPP_AHVRR issue 2.0, 19/08/2016, doi: 10.5676/EUM_SAF_CM/CLARA_AVHRR/V002, 2016b.

Page 7, line 3-4*: The size distributions do not depend on wavelength (line 3), but the phase functions do (line 4), so please shift "for the visible wavelength (0.6 μm)" after "phase functions". Please correct also the caption of Fig. 2.*

Corrected.

Page 7, line 4-5*: Please indicate in the text and/or in the figure where the cloudbow and glory features can be observed.*

Cloud bow and glory features manifest as peaks near 140° and in the backscattering direction, respectively. This is added in the revised manuscript (page 7, lines 20-21)

Page 7, Table 1*: Is there such a set of LUTs for every value of the surface albedo mentioned in the text? Please explain this.*

No, as explained earlier, radiative transfer calculations for three values of the surface albedo are used to derive cloud transmittance and hemispherical sky albedo, which are stored in the LUT, and allow the calculation of the cloud reflectance for any albedo of the underlying surface.

Page 8, line 4*: Please indicate in the text here and not only in the caption of Fig. 1 the details of the region coordinates.*

Added (page 9, lines 6-7).

Page 8, line 5*: Please mention which quantity has been used to assess "uniformity" of the cloud deck.*

By "uniformity" we mean high degree of spatial coverage. We have rephrased accordingly (page 9, line 7).

Page 8, line 8-10*: This argument, related to the different viewing conditions, also depends on the cloud field observed. If the Sc has dimensions that are anyway smaller than the spatial resolution of SEVIRI, only small differences might appear here.*

This is indeed the case in the updated results. Differences are larger in the continental case and only minor in the marine region (Fig. 3).

Page 8, line 10*: What does it mean that MSG-1 detected "more ice clouds"? Are there ice clouds during these days? Do they contribute to the cloud cover shown in Fig. 3? Are there ice clouds that MSG-3 does not detect and contribute to the retrieval results (Fig. 4 onward)? Are ice clouds maybe one of the reasons for the differences in cloud cover from MSG-1 and MSG-3? Which further factors might explain these differences?*

Examination of the retrieved cloud phase data showed that over the southeastern Atlantic between 12:30 and 17:00 UTC MSG-1 retrieved ice clouds covering 3-4% of the 5° × 5° study region, reaching 17% in 16:30 and 16:45 UTC. For the same time slots ice cloud cover from MSG-3 never exceeded 0.5%. Over the 4° × 4° continental region both satellites detected ice clouds covering between 10% and 20% from 14:00 UTC to 16:00 UTC and about 5% in other time slots. While these findings can explain results shown in Fig. 3, ice clouds did not contribute to later retrieval results, which were constrained to pixels where both satellites retrieved liquid clouds. Furthermore, in the revised manuscript, where both study regions are decreased to 2° × 2°, ice cloud coverage over the southeastern Atlantic for the same time slots from MSG-1 never exceeds 4%, while no ice cloud is detected from MSG-3. Over the 2° × 2° continental region, ice clouds never exceed 2% in either satellite retrieval. Hence, this statement was removed from the revised manuscript.

Page 8, line 14*: At this point of the manuscript it is not clear yet when the cloudbow and glory geometry occur, so please explain this in the text. Nevertheless, if you merge this figure with Fig. 4 or 12, as suggested above, this remark is superfluous.*

Our purpose here is not to highlight the cloud bow and glory time slots, but rather to mention that they are also included in the time range with high liquid cloud cover. This part was rephrased accordingly (page 9, lines 18).

Page 8, line 21*: In the MSG-1 curve in Fig. 3a there are discontinuities in the afternoon while the MSG-3 cloud cover is very smooth. Might they be caused by sunglint? Which possible effects might explain these differences otherwise?*

Figure 3 was updated based on the revised analysis and the reduced size of the study regions (2°×2°). Discontinuities in the MSG-1 curve are now much less pronounced. Sunglint conditions are included in CPP as a flag, and it was indeed found that these conditions were fulfilled for some pixels and time slots in late afternoon over the southeast Atlantic region with MSG-1. However, their effect on CPP retrievals would be significant only if clear-sky pixels were misinterpreted as cloudy. The good agreement between MSG-1 and MSG-3 cloud cover ensures that this is not the case here.

Page 10, line 6-7*: "with values increasing rapidly ..." ! Please explain.*

This increase in reflectances from MSG-1 in late afternoon, which is not present in MSG-3, should probably be attributed to a combination of the sun positioned low above the horizon and the viewing angle of MSG-1, which is larger than that of MSG-3. It should be noted however that, based on the CPP output, where no similar difference is found, these conditions are accounted for in the retrieval LUTs. This is clarified in page 12, lines 7-9 of the revised manuscript.

Page 10, line 10*: "different illumination conditions" ! please explain.*

Here we mean illumination *and viewing* conditions. We have rephrased accordingly (page 12, line 12).

Page 10, line 27*: Please mention the observation conditions that are shown here.*

The observation conditions (θ, θ_0 and Θ) are given in the revised Fig. 5 (for MSG-1: $\theta = 43.4°$, $\theta_0 = 55.7°$, $\Theta = 86.1°$; for MSG-3: $\theta = 22.7°$, $\theta_0 = 55.7°$, $\Theta = 134.1°$).

Page 11, line 1-3*: This is an interesting point and also not obvious since the reflectance observed by the satellite is affected by single and by multiple scattering at the same time. Thus it is not trivial to find a signature of the single scattering properties in this quantity. Please consider mentioning this aspect in the text.*

We agree with the reviewer and we have included this aspect in the text. We have also added that this LUT characteristic affects optically thin clouds only, where single scattering prevails (page 13, lines 7-11).

Page 11, line 9*: Please quantify "thin".*

Based on the LUT in Fig. 5a, $\tau < 4$ would be a rough quantification (included in page 13, line 18).

Page 11, line 15*: Is this assertion from Mayer et al. (2004) who used reflectances at 753nm also valid for other wavelengths? I think you can cite your plots as well to explain this.*

This part was rephrased to reflect the referee's suggestion (page 14, lines 1-2).

Page 12, line 9-11*: Could you please explain what you mean with this sentence, in particular with "their differences"?*

In the case of τ, where differences due to different size distributions appear only in cloud glory conditions (Fig. 7a), the sensitivity to v_e is clear. In the case of r_e, however, we have differences in both glory but also large irregularities in cloud bow conditions, and the glory from one satellite almost coincides with the cloud bow from the other. Hence, it is difficult to discern the sensitivity to v_e. This part is rephrased in the revised manuscript (page 15, lines 8-10).

Page 12, line 11*: What is meant with "This is due..."?*

We mean the difficulty to discern the sensitivity to v_e. This sentence has been rephrased (see also our reply to the previous comment).

Page 12, line 12-13*: If you "give up" your synergistic approach of using MSG-1 and MSG-3 you might consider showing results from only one satellite. This would make the next figures "lighter" and you can eventually mention that these results are confirmed (not shown) by the other satellite.*

While the reviewer's suggestion would indeed make the presentation of results "lighter", we opted to continue the analysis with both satellites. The main reason is that including a second satellite adds cases with different scattering angles, which can contribute to the analysis.

***Page 13, Fig. 7**: Why is the effect of the glory smaller for MSG-3?*

This difference should be attributed to the different maximum scattering angles: 176.4° for MSG-1 and 172.6° for MSG-3. An inspection of Fig. 6a, and especially the corresponding separation index values (Fig. S3 of the supplement) shows that indeed MSG-1 would be more prone to failures, and thus irregularities, than MSG-3. This is explained in the revised manuscript (page 17, lines 12-15).

***Page 14, line 7**: Please specify "significant effect" and put it in relation to the uncertainty of the r_e retrieval.*

The term "significant" here was not meant in a statistical sense, and was replaced by "strong" for more clarity. The retrieval uncertainties are analyzed in the revised manuscript as described in page 8, lines 8-14, and page 9, lines 1-2, and they are discussed in relation to our results throughout the manuscript.

***Page 14, line 8**: Please explain what you mean by "The effect on the glory is similar to the τ case".*

We mean that the effect of v_e on r_e in the glory is similar to the effect of v_e on τ in the glory. We have rephrased accordingly (page 17, lines 11-12).

***Page 14, line 14**: "which are flagged" as bad quality? As uncertain?*

As pixels where the pair of VIS and SWIR reflectances lies outside the Nakajima-King LUT. We have added this clarification (page 18, line 4).

***Page 15, line 10-11**: "... these distributions cannot capture the cloud glory adequately." Do you mean that such distributions do not show the glory effect or that Mie theory is not adequate for such distributions? The size parameter for 1 µm particles (small cloud droplet) at 1.6 µm is still 3.9 and even higher at 0.6 µm. Are you really sure that Mie theory is not suitable?*

We mean that in such distributions the cloud glory effect is much weaker, as can also be seen in Figs. 6b and 6c for phase functions at 0.6 µm and 1.6 µm, respectively. We have rephrased accordingly (page 18, line 19).

***Page 15, line 11**: "...adequately." Please add a reference.*

This part has been rephrased (see previous comment).

***Page 16, Fig. 10**: Why is v_e indiced variability spread over such a large time period, especially for MSG-1 (6-11 UTC)?*

This spread should be attributed to the different characteristics of the 3.9 µm phase function in the backscattering directions. Specifically, glory features are wider compared to smaller wavelengths (see e.g. Figs. 11a and 6b), covering a larger range of scattering angles, hence the variability will be spread over a larger time period. This is added in the relevant description of Fig. 10 (page 20, lines 19-21).

***Page 16, line 13**: Is the assertion about the 3.9 µm phase function separation for different v_e still valid if you rescale the plot (Fig. 11) as in Fig. 6? In principle, you should/could introduce a sort of phase separation index as in Cho et al. (2015) to quantitatively answer this question.*

Following the reviewer's suggestions, we introduced the Cho et al. (2015) phase separation index in our analysis. Index values at 172° scattering angle are indeed smaller in the 3.9 µm phase function compared to the 1.6 µm phase function (Figs. S5 and S7 of the supplement). This is also mentioned in the revision (page 20, lines 15-18).

***Page 17, Fig. 14**: Which "part of the results" is expected? Why for "an optically moderately thick" cloud? Please explain.*

This sentence has been rephrased for clarity (page 21, lines 14-15).

***Page 18, line 5**: "wider size distributions are expected": please give a reference.*

This expectation is based on the results of Miles et al. (2000). Added in page 22, line 4.

***Page 18, line 5-9**: The glory issue in the continental case should be investigated in the same detail as the marine one. It is not clear which features characterise the phase function at these higher angles (177-178°) that cannot be explained like for the 172° scattering angle in the marine case. By the way, a scattering angle plot for the continental case should be presented.*

This part has been expanded. The relevant phase function is now shown (Fig. 6b) along with the respective separation index (Fig. S3). Scattering angles for the continental case are also shown in revised Fig. 12.

***Page 20, Table 2**: Please add which cloud types (Sc, Cu...) have been investigated by Miles et al. (2000).*

Added in page 25, lines 22-24.

***Page 20, line 11**: What is meant by "In marine only clouds"?*

We meant "marine Sc clouds". We have rephrased accordingly (page 25, lines 25).

***Page 20, line 22**: Please explain/rephrase "further emphasized".*

Here we mean the fact that the conclusions drawn from the present study are similar to those from previous studies. We have rephrased this part for more clarity (page 26, lines 11-13).

Technical corrections

***Abstract**: The verbs should be in the present tense, e.g. "are analysed" instead of "were analysed".*

Done.

***Page 1, line 2**: "... (LWP), which is a crucial component..." ! marine low clouds are a crucial component, not LWP. Please rephrase.*

Rephrased.

***Page 1, line 9**: detection ! observation.*

Changed.

***Page 1, line 15**: "different underlying surfaces" ! please write land and ocean.*

Done.

***Page 1, line 13**: "Cloud_cci"!please write ESA's Climate Change Initiative (essential climate variables related to clouds) or something like this.*

Done.

***Page 1, line 15-16**: "more recent and advanced sensors provide high spatial and temporal resolution" ! "... spatial and/or temporal resolution"*

Changed.

***Page 1, line 20**: I think that the CALIPSO/CALIOP lidar and CloudSat/CPR should be shortly mentioned here.*

We did not mention CALIPSO/CALIOP and CloudSat/CPR since the focus is on passive imagers only.

***Page 1, line 21**: "routinely retrieved from passive VIS-IR" ! "routinely retrieved from e.g. passive VIS-IR" since also pure thermal algorithms exist, especially for cirrus clouds (e.g., Heidinger and Pavolonis, 2009; Holz et al., 2016; Minnis et al., 2016; Strandgren et al., 2017).*

We focus on the VIS-IR methods here. It is not relevant that cloud optical and microphysical properties are also retrieved from other wavelengths.

***Page 1, line 30**: "... biases reported..." ! please cite already here the papers you mention below.*

Done.

***Page 2, line 7**: "... not retrieved" ! at this place the sentence "While under most retrieval circumstances..." on line 15 would fit particularly well.*

The sentence was moved.

***Page 4, line 12**: The height above the equator could be omitted.*

Done.

***Page 4, line 19**: "diurnal basis" ! "hourly basis".*

Changed.

***Page 5, line 6**: "12 spectral channels between" ! "12 spectral channels in"*

Changed.

***Page 5, line 7**: Please mention also the HRV channel.*

Done.

***Page 5, line 7**: Please introduce the CCP algorithm in Sect. 2.2 and not here.*

This part was moved to the beginning of Sect. 2.2.

***Page 5, line 9**: "near wavelength" ! "centred at wavelength".*

We really mean 'near'. The central wavelength is not 0.6 μm but 0.635 μm. For clarity we mention the exact central wavelengths and the approximate values used further on in the paper in the revised manuscript (page 6, line 11).

***Page 5, line 13-14**: Please mention the operational calibration slopes to have an idea about the differences in calibration.*

We introduced the following phrase: 'These values can be compared with the corresponding operational calibration slopes of 0.0241, 0.0233, 0.0209, and 0.0236 mW m^{-2} sr^{-1} $(cm^{-1})^{-1}$, respectively.' (page 6, lines 6-7).

***Page 6, line 20**: "contained within" ! "filtered with"*

Changed.

***Page 7, line 1**: "approach" ! "selection".*

Changed.

***Page 7, line 5**: Please rephrase "along with differences..." as "but the details of the phase functions for these scattering situations depend on the effective variance".*

Rephrased.

Page 7, line 7*: 180 ! 180*°.

Corrected.

Page 7, Table 1*: The rows in the third column are not aligned with the rows in the second column, please correct.*

Corrected.

Page 7, Fig. 2b*: Please add "scattering angle" to the x axis title.*

Added.

Page 8, line 3*: "equinox" ! "vernal equinox".*

Added.

Page 8, line 7*: "spatial coverage" ! "cloud cover".*

Replaced.

Page 8, line 9*: "more clouds" ! "higher cloud cover".*

Replaced.

Page 8, line 9*: "over the continental region and less over the marine" ! "over the continental and less over the marine region w.r.t. MSG-1".*

Rephrased.

Page 8, line 11-12*: "their high spatial coverage with liquid clouds" ! "the high liquid cloud cover".*

Rephrased.

Page 9, Fig. 4a*: Please add "scattering angle" to the y axis title.*

Added.

Page 10, line 13*: "were based" ! "are based".*

Changed.

Page 10, line 24*: "showed" ! "shows".*

Changed.

Page 10, line 27*: "same" ! "corresponding" or "appropriate".*

Changed.

Page 10, line 27*: "the LUT now covers" ! "the LUT for MSG-1 covers".*

Rephrased.

Page 11, line 15*: "the phase function" ! "the phase function at 1.6 µm".*

Added.

Page 11, line 16*: "the distance" ! "the angular distance".*

Added.

Page 11, line 18*: "range" ! "intensity".*

Replaced.

Page 11, Fig. 6*: Please plot larger ticks on the y axes.*

Done.

Page 15, line 6*: "increase" ! "increases".*

Corrected.

Page 18, line 3*: "will affect" ! "affects".*

Changed.

Page 19, line 9*: "decreased flagged pixels" ! "decreased numbers of flagged pixels".*

Changed.

Mayer et al. (2015)*: Should read Mayer et al. (2004).*

Corrected.

Wood and Hartmann (2005)*: Should read Wood and Hartmann (2006).*

Corrected.

References

Seethala, C., Meirink, J. F., Horváth, Á., Bennartz, R., and Roebeling, R.: Evaluating the diurnal cycle of South Atlantic stratocumulus clouds as observed by MSG SEVIRI, Atmos. Chem. Phys., 18, 13283-13304, doi: 10.5194/acp-18-13283-2018, 2018.

Stengel, M., Stapelberg, S., Sus, O., Schlundt, C., Poulsen, C., Thomas, G., Christensen, M., Carbajal Henken, C., Preusker, R., Fischer, J., Devasthale, A., Willén, U., Karlsson, K.-G., McGarragh, G. R., Proud, S., Povey, A. C., Grainger, R. G., Meirink, J. F., Feofilov, A., Bennartz, R., Bojanowski, J. S., and Hollmann, R.: Cloud property datasets retrieved from AVHRR, MODIS, AATSR and MERIS in the framework of the Cloud_cci project, Earth Syst. Sci. Data, 9, 881-904, doi: 10.5194/essd-9-881-2017, 2017.

Sensitivity of liquid cloud optical thickness and effective radius retrievals to cloud bow and glory conditions using two SEVIRI imagers

Nikos Benas[1], Jan Fokke Meirink[1], Martin Stengel[2], Piet Stammes[1]

[1]Royal Netherlands Meteorological Institute (KNMI), De Bilt, The Netherlands
[2]Deutscher Wetterdienst (DWD), Offenbach, Germany

Correspondence to: Nikos Benas (benas@knmi.nl)

Abstract. Retrievals of cloud properties from geostationary satellite sensors offer extensive spatial and temporal coverage and resolution. The high temporal resolution allows the ~~detection~~ observation of diurnally resolved cloud properties. However, retrievals are sensitive to varying illumination and viewing geometries, including cloud glory and cloud bow conditions, which can lead to irregularities in the diurnal data record. In this study, these conditions and their effects on liquid cloud optical thickness and effective radius retrievals a~~we~~re analyzed using the Cloud Physical Properties (CPP) algorithm. This analysis i~~wa~~s based on the use of SEVIRI reflectances and products from Meteosat-8 and -10, which are located over the Indian and Atlantic Ocean, respectively, and cover an extensive common area under different viewing angles. Comparisons of the retrievals from two full days, over ~~different underlying surfaces (~~ocean~~/~~ and land~~,)~~ and using different spectral combinations of visible and shortwave-infrared channels a~~we~~re ~~also~~ performed, to assess the importance of these factors in the retrieval process. The sensitivity of the cloud bow and glory related irregularities to the width of the assumed droplet size distribution ~~wa~~is analyzed by using different values of the effective variance of the size distribution. The results suggest for marine stratocumulus clouds an effective variance of around 0.05, which implies a narrower size distribution than typically assumed in satellite-based retrievals. For ~~a~~ the case with continental clouds a broader size distribution (effective variance around 0.15) ~~wa~~is obtained. This highlights the importance of appropriate size distribution assumptions and provides a way to improve the quality of cloud products in future climate data record releases.

1 Introduction

Low warm clouds contribute a large part of the overall cloud effects and feedbacks on the climate system (Zhou et al., 2016). Forming uniform decks, especially over large oceanic areas around the globe, they increase the planetary albedo and exert a cooling effect in the Earth's radiative balance (Wood, 2012).

Optical and microphysical properties of liquid clouds, specifically optical thickness (τ) and effective radius (r_e), are important for the estimation of cloud-radiation interactions and the consequent effects on the atmospheric radiation budget.

They are also used for the calculation of the cloud droplet number concentration (CDNC), which is a key parameter for the assessment of aerosol-cloud interactions (Grosvenor et al., 2018), and the cloud liquid water path (LWP) of marine low clouds, which ~~is~~ are a crucial component of the water cycle (Wood and Hartmann, 2006~~5~~). Furthermore, climate models rely on the measurements or retrieval of these cloud properties for the evaluation of their relevant parameterizations (e.g. Pincus et al., 2012).

These characteristics highlight the importance of continuous monitoring of clouds and their properties, which on a global scale is possible only through satellite observations. In fact, during the last decades, substantial advances have been made regarding the continuous and reliable retrieval of cloud properties. Cloud property data records derived from satellite-based passive visible-infrared (VIS-IR) imagers start already in the early 1980s, based on Advanced Very High Resolution Radiometer (AVHRR) measurements from polar orbiting satellites, e.g. the Satellite Application Facility on Climate Monitoring (CM SAF) Cloud, Albedo and Surface Radiation dataset from AVHRR data - second edition (CLARA-A2, Karlsson et al., 2017) and the Pathfinder Atmospheres - Extended (PATMOS-x, Heidinger et al., 2014) data records; combinations of measurements from polar orbiting sensors, e.g. the ~~Cloud_cci~~ESA's Climate Change Initiative cloud data records, which are based on AVHRR, MODIS, ATSR-2 and AATSR (Stengel et al., 2017); and measurements from polar and geostationary satellites, e.g. the International Satellite Cloud Climatology Project (ISCCP) data set (Young et al., 2018). Additionally, more recent and advanced sensors provide high spatial and/or temporal resolution in more spectral channels, also increasing the number and reliability of cloud properties retrieved. Examples of such sensors include the Moderate Resolution Imaging Spectroradiometer (MODIS) and the homonymous cloud data set (Platnick et al., 2017), and the Spinning Enhanced Visible and Infrared Imager (SEVIRI) and the corresponding Cloud property dAtAset using SEVIRI - second edition (CLAAS-2) data record (Benas et al., 2017).

Cloud optical and microphysical properties are presently routinely retrieved from passive VIS-IR satellite imager measurements, basically following the "Nakajima-King" approach (Nakajima and King, 1990). This retrieval principle is based on the combination of a visible/near-infrared channel in which clouds are non-absorbing and the reflectance is primarily a function of τ and a shortwave-infrared (SWIR) channel in which clouds are absorbing and the reflectance is primarily a function of r_e. Methods utilizing this principle are currently applied to all sensors with an appropriate combination of channels.

Despite the continuous advancements in both satellite sensors and retrieval algorithms, challenging issues remain. One of them is the ~~biases~~ problematic retrievals reported in liquid cloud optical and microphysical properties, associated with specific illumination conditions (Zeng et al., 2012; Cho et al., 2015; Liang et al., 2015). These conditions include the backscattering directions, where the cloud glory effect is manifested, and scattering angles close to 140°, where the cloud bow effect, which is the equivalent of the rainbow created by cloud droplets, appears (Können, 2017). Retrieval failures and biases in τ and r_e may occur under these conditions for different reasons and have been reported for cloud glory and cloud bow in MODIS (Cho et al., 2015) and cloud bow in MODIS and the Multi-angle Imaging Spectroradiometer (MISR, Liang et al., 2015), while angular biases under the same conditions were also found in retrievals from Polarization and Directionality of the Earth's Reflectances (POLDER) observations (Zeng et al., 2012).

Another issue in cloud optical properties retrieval, which relates to the cloud glory effect, is the width of the cloud droplet size distribution assumed in the retrieval process. This width is usually represented by the effective variance (v_e) of the size distribution or other equivalent measures, e.g. the shape parameter μ (Petty and Huang, 2011). In case of passive satellite sensors that measure total reflectance, v_e is not retrieved; a constant value is instead assumed and used for the retrieval of τ and r_e of all liquid clouds. While under most retrieval circumstances the sensitivity of τ and r_e to v_e is low, this is not the case for special illumination geometries, as was shown e.g. in Mayer et al. (2004) for the cloud glory conditions. Typical v_e values used in satellite-based retrievals lie between 0.10 and 0.15. The former is the value used in MODIS Collection 6, ISCCP-H (Rossow, 2017) and PATMOS-x (Walther and Heidinger, 2012), while in the Cloud_cci data records v_e equals 0.11 (McGarragh et al., 2018). For the CLARA-A and CLAAS records v_e equal to 0.15 is assumed (Karlsson et al., 2013; Stengel et al., 2014; Karlsson et al., 2017; Benas et al., 2017). In MODIS Collection 5, a standard deviation of a lognormal size distribution equal to 0.35 was used (Liang et al., 2015), which corresponds to a v_e equal to 0.13 (Nakajima and King, 1990). Studies including in situ measurements, however, suggest a significantly wider range of v_e values, depending on cloud types, regions (marine or continental, see e.g. Miles et al., 2000) but also for the same cloud type (Igel and Van den Heever, 2017). ~~While under most retrieval circumstances the sensitivity of τ and r_e to v_e is low, this is not the case for special illumination geometries, as was shown e.g. in Mayer et al. (2015) for the cloud glory conditions.~~

In the present study we analyze irregularities in the diurnal evolution of retrieved cloud optical and microphysical properties (τ and r_e), appearing near the cloud glory and cloud bow geometries, and their sensitivity to the width of the assumed cloud droplet size distribution. For the analysis of the diurnal variability of optical properties, we use data from SEVIRI on board geostationary satellites Meteosat-8 and -10, and the Cloud Physical Properties (CPP) retrieval algorithm (Benas et al., 2017; Roebeling et al., 2006), used in the production of CLARA-A2 and CLAAS-2 data records. Cloud glory and cloud bow, and the ensuing irregularities in the retrievals, occur in specific time slots depending on the region and the season. Hence, their study is necessarily limited to small areas and specific days, since extensive spatial or temporal averaging would diminish their effects. We focus ~~primarily~~ on ~~a~~ two regions and two characteristic days, one over the southeastern Atlantic and ~~one characteristic day~~ the other inland over southeastern Africa, at similar latitudes. Each of ~~T~~these~~is~~ regions is scanned by the two SEVIRI sensors of both Meteosat satellites under different illumination conditions, so that possible effects near the cloud glory and near the cloud bow occur in the two retrievals at different times. In this way, and by comparing the diurnal evolution of the retrieved optical properties from the two satellites, we can assess the effects of these illumination conditions on the retrievals. ~~While in principle the retrieval algorithm should compensate for the different viewing and illumination~~

~~geometries, and the two products should agree under any circumstances, we show that this is not the case by monitoring the diurnal evolution of the retrieved optical properties.~~

The sensitivity of these effects to the width of the assumed size distribution is analyzed by performing retrievals using different values of the corresponding v_e. Intercomparisons of the products derived from these retrievals help in the assessment of their sensitivity and highlight the importance of selecting the appropriate value of v_e. Apart from this analysis, three additional retrievals are performed; one over the same region, but using a different spectral combination of visible and SWIR channels, and two over a land area of southern Africa, using both spectral combinations. Corresponding comparisons of different underlying surfaces (ocean/land) and different channel retrievals provide further insights ~~on~~ into the relative importance of these factors in the retrieval process.

The combined use of retrievals from the two sensors to analyze the effects of cloud bow and cloud glory is based on the assumption that retrievals would otherwise be the same. This is not always the case, since other factors can cause differences between retrievals from the same algorithm applied to the same sensor on different platforms. These factors include, among others, shadow and other 3D effects, partially cloudy pixels and cloud inhomogeneity, surface effects, and misidentification of clouds (e.g. thin cirrus) or cloud phase. Here we show that the aforementioned assumption is valid in the marine case, while over the land area differences are found. However, the simultaneous analysis from both satellites is still valuable, in terms of verifying common effects from two different points of view.

In the following section we describe the two Meteosat satellites and the CPP retrieval algorithm in more detail, along with the data used and the way these were processed. Section 3 includes the results, focusing first on the retrieval algorithm input and output over the ~~South~~ southeastern Atlantic region, their characteristics due to different illumination conditions (Sect. 3.1) and their dependence on the width of the assumed size distribution (Sect. 3.2). Comparisons between retrievals from different spectral pairs and over different underlying surfaces are presented in Sects. 3.3 and 3.4, followed by the discussion and conclusions.

2 Data and M~~m~~ethodology

2.1 Satellites

EUMETSAT operates four Meteosat Second Generation (MSG) satellites, namely Meteosat-8, -9, -10 and -11 (also referred to as MSG-1, -2, -3 and -4, respectively), ~~.~~ a~~A~~ll ~~four are~~ positioned in geostationary orbit~~, about 35786 km above the equator~~. In September 2016 MSG-1 was nominally positioned at 41.5° E longitude, covering mainly Africa and the Indian ocean, and in early 2017 the Indian Ocean Data Coverage (IODC) service became operational. MSG-3 was the primary operational satellite for Africa, Europe and the Atlantic Ocean, nominally positioned at 0° longitude, between January 2013 and

February 2018. The areas covered by MSG-1 and MSG-3 have a large overlap (see Fig. 1), comprising Africa, Europe, the Middle East and large oceanic regions, which offers new opportunities for synergistic usage of data from the two satellites.

It should be noted that the two satellites deviate from their nominal positions ~~on a diurnal basis~~over the course of a day. In the period considered in this study (March 2017), this deviation is most pronounced in the latitude of MSG-1, which ranges between approximately 5° S and 5° N on a 24-hour basis. This deviation alters the viewing geometry and estimated scattering angles, thus also affecting the retrieved optical properties. To avoid possible consequent misinterpretations, information on the exact position of each satellite, available on a 15-minute time slot basis, was included in the retrieval process.

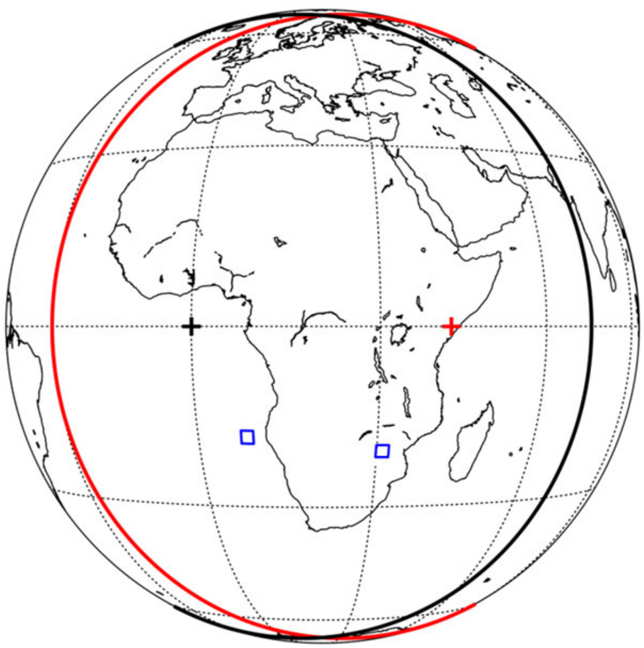

Figure 1: The overlap area created by the disks of MSG-1 (red line) and MSG-3 (black line). The red and black crosses show the corresponding nominal sub-satellite points. The blue rectangles show the ~~primary~~ study regions west of the African coast (16.5°-~~20~~18.5° S, 7.5~~6~~°-9.5~~11~~° E) and ~~the secondary~~ in the southern parts of Zimbabwe and Mozambique (19~~8~~°-21~~2~~° S, 30~~29~~°-32~~3~~° E).

SEVIRI is one of the main instruments on board the MSG satellites. It observes the Earth in 11~~2~~ spectral channels ~~between~~ from the visible ~~and~~ to the thermal infrared and one high resolution broad-bandwidth channel in the visible (HRV), acquiring measurements every 15 minutes at 3 km nadir resolution (1 km for the HRV). ~~The CPP algorithm uses measurements from one visible and one SWIR channel to retrieve τ and r_e. For SEVIRI, this is achieved by combining the channel near~~

~~wavelength λ = 0.6 μm with either the 1.6 μm or the 3.9 μm channel (CM SAF, 2016).~~ To ensure a valid intercomparison between MSG-1 and MSG-3 reflectances and retrievals, calibration of SEVIRI shortwave channels on both satellites was performed using Aqua MODIS Collection 6 reflectances as a reference, instead of the operational EUMETSAT calibration. The approach is described in Meirink et al. (2013) and was extended in this study to include 2017. This yielded calibration slopes of 0.0267, 0.0229, 0.0235, and 0.0229 mW m^{-2} sr^{-1} (cm^{-1})$^{-1}$ for the MSG-1 0.6 μm, MSG-1 1.6 μm, MSG-3 0.6 μm, and MSG-3 1.6 μm channels, respectively. These values can be compared with the corresponding operational calibration slopes of 0.0241, 0.0233, 0.0209, and 0.0236 mW m^{-2} sr^{-1} (cm^{-1})$^{-1}$, respectively.

2.2 Retrieval Method

The CPP algorithm uses measurements from one visible and one SWIR channel to retrieve τ and r_e. For SEVIRI, this is achieved by combining the channel near wavelength λ = 0.6 μm with either the 1.6 μm or the 3.9 μm channel (CM SAF, 2016a; corresponding central wavelengths are 0.635 μm, 1.64 μm and 3.92 μm, respectively). ~~The~~ CPP ~~algorithm~~ requires a cloud mask, and several cloud top properties as input. The cloud mask as well as cloud top height and temperature are obtained using the Satellite Application Facility for Nowcasting (NWC SAF) GEOv2016 software package (NWC SAF, 2016; Derrien and Le Gléau, 2005). The cloud top phase retrieval is based on a modified version of the Pavolonis et al. (2005) algorithm, as described in Benas et al. (2017). In this study only liquid phase clouds are considered. The physical principle of the CPP approach was described in Nakajima and King (1990). CPP ~~and~~ is presently used ~~for the retrieval of cloud optical and microphysical properties from~~with various satellite imagers, ~~. It relies on the dependence of the cloud reflectance in a visible (non-absorbing) channel mainly on τ, and that in a SWIR (absorbing) channel on r_e. These different characteristics render possible~~ for the simultaneous retrieval of τ and r_e by comparison with simulated cloud reflectances in the visible and SWIR under different illumination conditions.

For the radiative transfer calculations, a two-parameter gamma size distribution of liquid cloud droplets is assumed, given in Hansen (1971) and also described in Petty and Huang (2011):

$$n(r) = N_0 r^{\frac{1-3v_e}{v_e}} \exp\left(\frac{-r}{r_e v_e}\right) \quad (1)$$

The constant N_0 is provided in Hansen (1971) but is not required here, since the retrieval algorithm is based on normalized quantities. Mie scattering calculations are performed using a Mie code (De Rooij and Van der Stap, 1984), whereby the scattering matrix is calculated and provided in terms of generalized spherical functions. This output is then used as input for the multiple scattering calculations based on the Doubling-Adding KNMI (DAK) radiative transfer model (De Haan et al., 1987; Stammes, 2001), for the simulation of top-of-atmosphere (TOA) reflectances of clouds in a Rayleigh atmosphere for different channels, which are stored in a lookup table (LUT; see below for its layout). The reflectances R are defined as:

$$R = \frac{\pi I}{E_0 \cos\theta_0} \quad (2)$$

where I is the radiance measured by the satellite in a specific channel, E_0 is the downwelling solar irradiance at TOA ~~contained~~ filtered with~~in~~ the channel's spectral response function and θ_0 is the solar zenith angle. Using radiative transfer calculations for three values of the surface albedo, the reflectances can be calculated for the actual surface albedo, which is assumed to be constant over ocean (0.05 in the 0.6 and 1.6 µm channels, and 0.02 in the 3.9 µm channel) and obtained from MODIS-based climatologies over land (Greuell et al. (2013) at 0.6 and 1.6 µm and Seemann et al. (2008) at 3.9 µm). The measured reflectances are corrected for absorption by atmospheric gases, of which concentrations are obtained from the European Centre for Medium Range Weather Forecasting (ECMWF) Integrated Forecasting System (IFS) model (water vapour and ozone) or from climatologies (other trace gases). In case of the 3.9 µm channel, the measurement is further corrected for a contribution of thermal emission based on the IFS surface temperature and the retrieved cloud top temperature (CM SAF, 2016b). A match between the measurements and the LUT of simulated reflectances is then sought, yielding the cloud optical properties τ and r_e. Uncertainties of the retrieved values are estimated based on a 3% relative error in the reflectances. More details on the retrieval algorithm can be found in CM SAF (2016a).

To assess the sensitivity of the optical properties retrieval to the width of the liquid droplets size distribution, multiple Mie and DAK runs were performed, for the creation of seven LUTs. Each LUT corresponds to a different size distribution width, represented by a different value of v_e. The seven values of v_e were ~~selected~~ determined following the ~~approach~~ selection of Arduini et al. (2005) and their typical reported range (0.01-0.30, see also Miles et al., 2000; Igel and Van den Heever, 2017). Figure 2 shows the corresponding seven size distributions ~~for the visible wavelength (0.6 µm) and~~ for r_e = 12 µm (Fig. 2a) along with the scattering phase functions for the visible wavelength (0.6 µm) resulting from the Mie calculations (Fig. 2b). Cloud bow and glory features are apparent in all phase functions as peaks near 140° and in the backscattering direction, respectively, but the details of the phase functions for these scattering situations depend on the effective variance~~along with differences in their shapes especially near the cloudbow and in the backscattering directions~~. Each LUT contains simulated reflectances at the required wavelengths for various values and ranges of θ_0, the viewing zenith angle (θ), the relative azimuth angle ($\Delta\phi = 180°$ - $|\phi - \phi_0|$), τ and r_e. Table 1 summarizes these LUT characteristics.

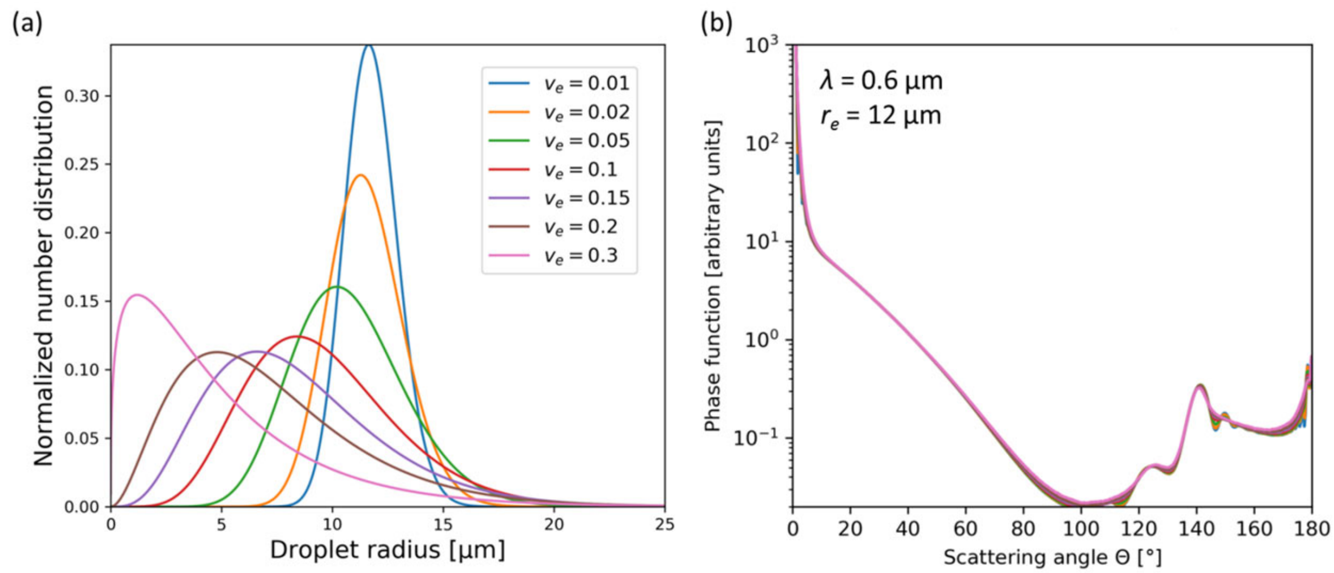

Figure 2: Normalized droplet size distributions for ~~λ = 0.6 µm and~~ r_e = 12 µm, for the seven values of effective variance v_e used in the Mie and DAK calculations (a), and corresponding scattering phase functions for λ = 0.6 µm derived from Mie calculations (b).

Table 1. Values and numbers of points of the variables comprising the five dimensions of the cloud reflectance LUTs. Each value of effective variance (v_e, last row) corresponds to a different LUT.

Variable	Values	Number of points
$\cos(\theta_0)$	0.099-1 (θ_0: 0-84.3°)	73, Gauss-Legendre points
$\cos(\theta)$	0.099-1 (θ: 0-84.3°)	73, Gauss-Legendre points
$\Delta\phi$	0-180°	91, equidistant
τ	0 and 0.25-256	22, equidistant in $\log(\tau)$
r_e	3-34 µm	8, equidistant in $\log(r_e)$
v_e	0.01, 0.02, 0.05, 0.10, 0.15, 0.20, 0.30	7

The pixel-based uncertainties were propagated in the calculation of spatial averages, using the methodology described in Stengel et al. (2017) for the propagation of uncertainty estimates from level 2 to level 3 products. This approach assumes bias-free Gaussian distributions for both the retrieved variables and their uncertainties, and estimates the eventual uncertainty depending on the level of correlation among level 2 uncertainties. In our case, while the pixel-based retrieval is performed assuming zero uncertainty correlation between adjacent pixels, some correlation should be expected. Considering this, we used an uncertainty correlation of 0.1 in our estimates, which was also used in Stengel et al. (2017). In order to compare the sensitivity of retrievals to v_e with corresponding uncertainties of these retrievals, we estimated the mean and standard deviation of the assumed Gaussian distributions of uncertainties for the two extreme retrieval cases in terms of ν_e (ν_e = 0.01 and ν_e = 0.30), and assessed their level of overlap. Hence, lower overlap indicates higher sensitivity of the retrieval to ν_e.

2.3 Selection of study areas and days

Using the different LUTs, liquid cloud τ and r_e were retrieved from MSG-1 and MSG-3 for two selected days and regions. Specifically, days near the vernal equinox were chosen so that the sun passed over the satellite, yielding glory viewing conditions. Subsequently, two study regions (one over ocean at 16.5°-18.5° S, 7.5°-9.5° E and one over land at 19°-21° S, 30°-32° E, see Fig. 1) were selected based on their high degree of spatial coverage with liquid clouds ~~deck uniformity~~ during specific days in 2017. For the oceanic region the CPP retrieval was performed for March 7, 2017, while for the land region the day selected was March 20, 2017. The CPP retrievals were performed separately for the pairs of channels 0.6 µm - 1.6 µm and 0.6 µm - 3.9 µm. Figure 3 shows the ~~spatial~~ cloud cover~~age~~ of the two areas with liquid clouds during the days selected. Based on the different viewing conditions, and the fact that larger viewing angles lead to larger cloud fractions retrieved, MSG-3 should yield ~~more~~ higher cloud cover~~s~~ over the continental ~~region~~ and ~~less~~ lower over the marine region compared to MSG-1 (see also Fig. 1). ~~The counterintuitive results in the latter case should be attributed to more ice clouds detected by MSG-1.~~ This is indeed the case over the continental region, while the good agreement between the two satellites over the marine region should probably be attributed to its almost complete coverage with liquid clouds. ~~While the reason for this difference is not obvious, the sizes of the two areas (5°×5° and 4°×4°) and t~~Thei~~r~~ high ~~spatial coverage with~~ liquid cloud cover~~s~~ throughout these days~~,~~ ensures the calculation of meaningful statistics of the retrieved cloud properties. In fact, liquid clouds cover more than 80% of these areas during the days selected, ~~and especially in~~including the cloud bow and glory time slots. It should be emphasized here that all results presented onward were based on pixels where both satellites retrieved liquid clouds, and where θ_0 was within the range defined in Table 1. The latter limitation explains the missing data in early morning and late afternoon.

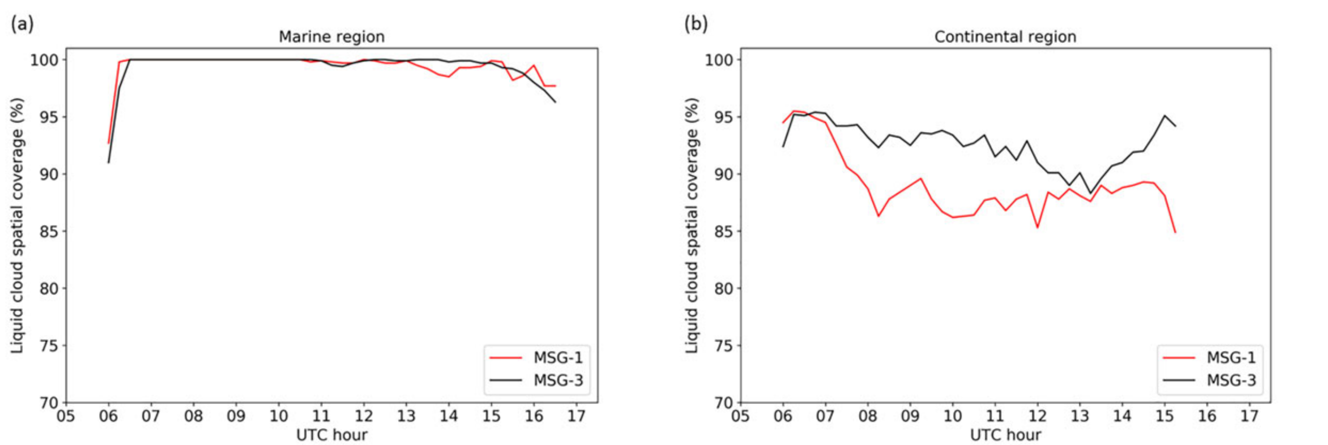

Figure 3: Spatial coverage (%) of the marine (a) and continental (b) regions with liquid clouds during March 7, 2017 and March 20, 2017, respectively, estimated separately from MSG-1 (~~black~~ red lines) and MSG-3 (~~red~~ black lines). The regions are indicated in Fig. 1.

Furthermore, although some afternoon time slots in MSG-1 could possibly be affected by sunglint conditions over the southeastern Atlantic, the good agreement between the two satellites during these time slots ensures that possible sunglint effects do not interfere with the results.

3 Results

3.1 Irregularities in the CPP diurnal cycle

Figure 4 shows the spatially averaged reflectances of the 0.6 µm and 1.6 µm channels used as input to the CPP algorithm over the southeastern Atlantic on March 7, 2017, separately from MSG-1 and MSG-3. Reflectances were averaged only over pixels with liquid cloud phase retrieved from CPP, to be directly comparable with the CPP output. Th~~e corresponding CPP~~is output, comprising spatially averaged τ and r_e values, is ~~also~~ shown, revealing a decreasing τ during the day (Fig. 4d), combined with a relatively constant r_e (Fig.4f).~~-~~ While this decrease in τ over the region is typical for this marine Sc deck, this is not the case for r_e, which typically also decreases (Seethala et al., 2018). Scattering angles, averaged over all pixels in the study region from the two satellites during this day, are shown in Figs. 4a and 4b, along with dotted and dashed vertical lines which highlight the ~~cloud glory and cloud bow~~ geometries near cloud glory and cloud bow (maximum values and 140° scattering angles, respectively). Scattering angles (Θ) are computed from θ_0, θ and $\Delta\varphi$ based on:

$$\Theta = \cos^{-1}(\sin\theta_0 \sin\theta \cos\Delta\varphi - \cos\theta_0 \cos\theta) \quad (3)$$

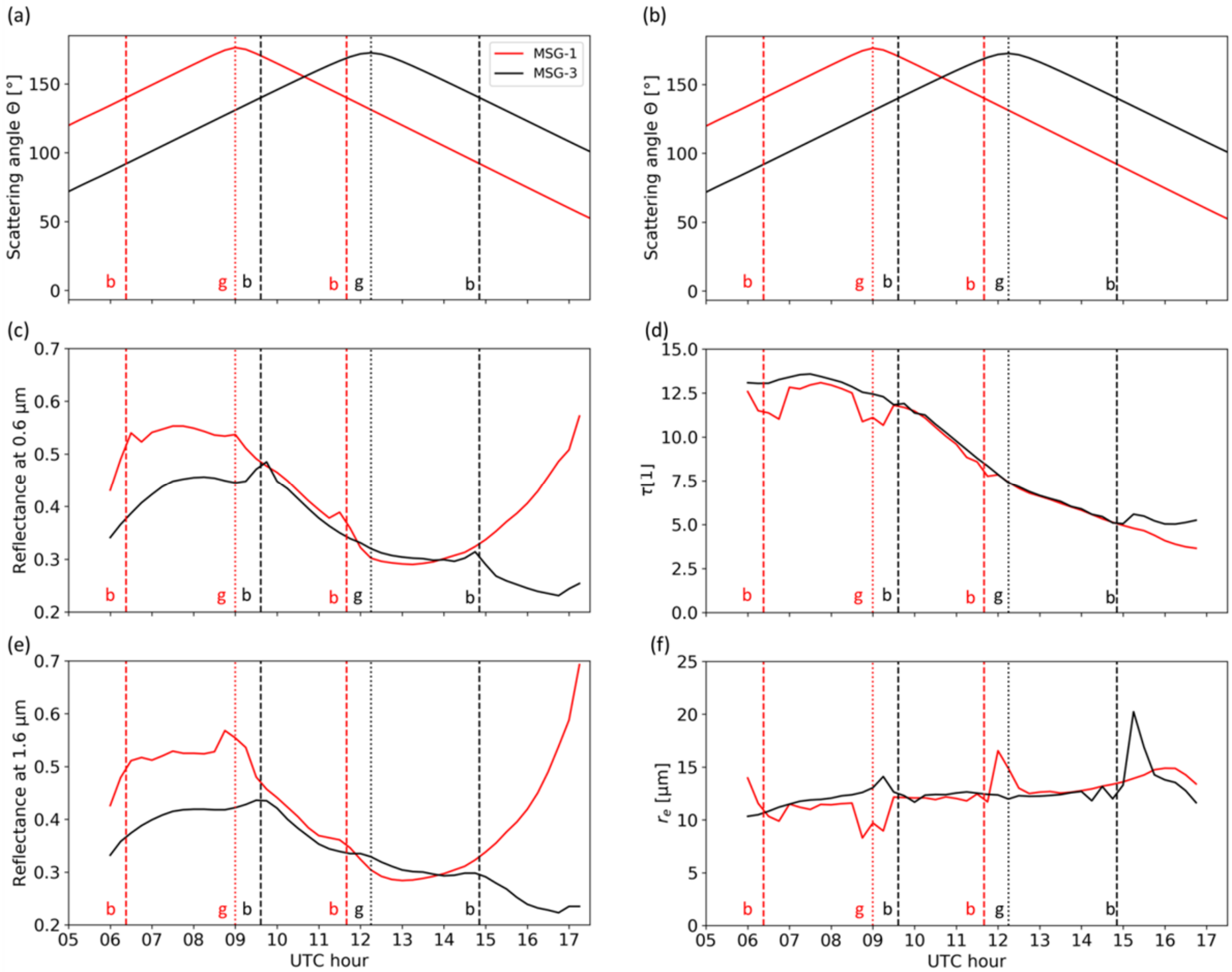

Figure 4: Diurnal evolution of average cloudy-sky reflectances observed from SEVIRI at 0.6 µm (c) and 1.6 µm (e) and CPP output τ (d) and r_e (f) over the southeastern Atlantic region on March 7, 2017. Scattering angles (a, b) are shown twice for visualization purposes. All data are shown separately for MSG-1 (red lines) and MSG-3 (black lines). The CPP output is based on retrievals with v_e = 0.15. Dotted vertical lines correspond to the maximum scattering angles, highlighting the cloud glory region, while dashed vertical lines are drawn at 140° scattering angles, roughly the cloud bow regions. Letters "b" and "g", corresponding to cloud bow and glory, respectively, are included next to the vertical lines to facilitate distinction.

It should be noted that the exact cloud bow angle varies with particle size. Nevertheless, it always lies around 140° (see also Fig. 2b), hence this angle was chosen here for visualization purposes. Furthermore, the glory does not necessarily coincide with the maximum scattering angle depicted in the cases plotted here. However, the angular distance between adjacent time slots (~3°), ensures that cloud glory conditions will occur (perhaps more than once) close to this maximum. The spatial averaging of pixels with slightly different scattering angles in the same time slot also introduces an uncertainty in the value of Θ. For an area size of 2° × 2°, as in our case, the typical range of scattering angle values is about 0.4°. This is narrow enough to ensure no "interference" between adjacent time slots, but also regarding phase function characteristics discussed later. Both cloud glory and cloud bow are apparent as irregularities in the diurnal evolution of reflectances, especially in the visible channel, whereas their effect is partially smoothed in the SWIR. The cloud glory irregularity appears around the maximum scattering angle for that day and region, which is about 176.4~~2~~° for MSG-1 and 172.6° for MSG-3. Cloud bow irregularities, on the other hand, occur in scattering angles close to 142°. Large discrepancies between MSG-1 and MSG-3 reflectances appear late in the afternoon, with values increasing rapidly for low scattering angles. This difference should probably be attributed to the combined large θ_0 and θ for MSG-1, but it does not appear to affect the corresponding retrievals.

Despite the possible differences in reflectances measured from the two sensors over the same area and time slot, which should be attributed to the different combinations of illumination and viewing conditions, the retrieval algorithm should in principle compensate for these and ideally produce the same results, which correspond to the real conditions examined from two different angles. In practice, however, this is hardly ever achieved, with many possible reasons contributing to eventual differences, as mentioned in the Introduction. Figures 4d and 4f show the retrieved τ and r_e separately from MSG-1 and MSG-3. These retrievals ~~were~~ are based on v_e = 0.15, which is the value used in the CLAAS-2 CPP version. For both satellites, apparent irregularities are centered on the cloud glory in both τ and r_e, with most pronounced discrepancies for r_e. It appears, however, that in the cloud bow time slots retrievals are rather normal, with big differences occurring in r_e for smaller scattering angles, namely close to 134~~2~~°. The very good agreement between the two satellites in other time slots suggests that other factors causing differences in retrievals do not play a substantial role here.

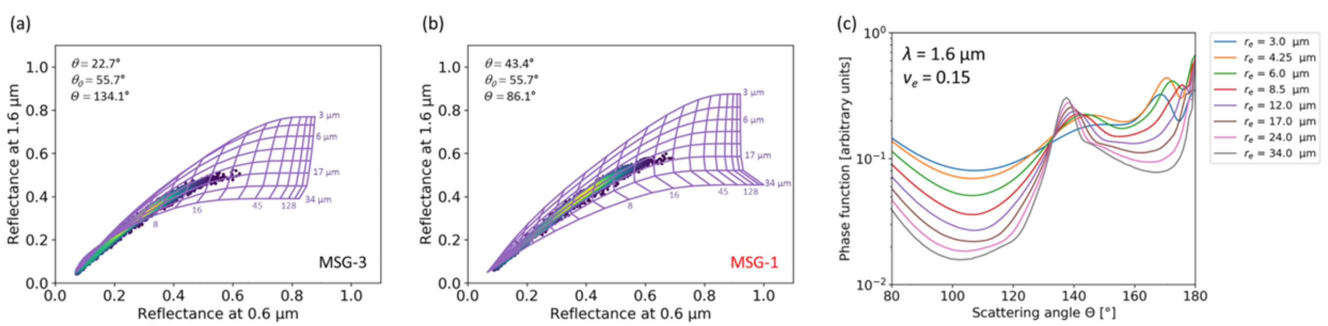

Figure 5: Density p~~P~~lots of (atmospheric absorption corrected) reflectance observations from cloudy pixels and corresponding retrieval LUTs for the 15:15 UTC time slot in March 7, 2017 over the southeastern Atlantic, separately for MSG-3 (a) and MSG-1 (b). Dark blue to yellow colors show increase in the density of points. (c) Phase functions at 1.6 µm wavelength used in the radiative transfer calculations for the eight r_e values of the LUTs, assuming v_e = 0.15.

Further analysis shows~~ed~~ that the cloud bows~~e~~ features are caused by a large number of observations falling outside the LUT, specifically below, leading to r_e retrievals at its highest value (34 μm). This is illustrated in Fig. 5a, which shows the ~~scatter~~ density plot of cloud reflectances observed from MSG-3 at 0.6 μm and 1.6 μm at 15:15 UTC, when r_e peaks (see Fig. 4f), overplotted with the LUT for the same illumination conditions, which was used in the retrieval. For comparison purposes, the ~~same~~ corresponding plot is shown for MSG-1 during the same time slot (Fig. 5b). It is apparent that the LUT ~~now~~ for MSG-1 covers the observations more adequately, leading to more reasonable r_e retrievals, judging from comparisons~~ed~~ with~~to~~ adjacent time slots. The reflectance observed by the satellite is affected by single and by multiple scattering at the same time. Hence, while it is not trivial to find a single scattering signature here, ~~T~~the origin of this LUT inadequacy, occurring for scattering angles around 133~~2~~°, can probably be traced back to the scattering phase functions used for the LUT calculations. The fact that this LUT characteristic affects optically thin clouds only, where single scattering occasions are more pronounced, supports this explanation. Figure 5c shows the shape of these phase functions in the scattering angle range 80°-180° for all eight r_e values used in the LUT. The overlap of all the phase functions near 133~~2~~° provides no information on the r_e, and leads to the corresponding "collapse" in the left part of the LUT (Fig. 5a). A similar collapse occurs for scattering angles slightly larger than those of the cloud bow but their effect on the averaged retrievals is far less severe. On the other hand, scattering angles in the MSG-1 case lie around 86°, where Figs. 5b and 5c show that r_e is adequately retrievable. These characteristics in the phase functions were also reported for similar scattering angles in the case of MODIS where failure rates also increased (Cho et al., 2015). It should be noted, however, that this inadequacy is characteristic of optically thin clouds only ($\tau < 4$ in the case of Fig. 5a). It is obvious from the LUT shape in Fig. 5a that for clouds with higher τ, where multiple scattering prevails, r_e can be adequately retrieved.

To quantify the way that specific characteristics of the bulk scattering phase functions affect the failure rates in MODIS cloud optical properties retrievals, Cho et al. (2015) defined the phase function separation index (PS index) as the ratio between the mean and the standard deviation of phase functions at a given scattering angle for all r_e values used in the MODIS LUT. In this way, high values of PS, occurring where phase functions collapse, coincide with high rates of failed retrievals. Following the same method, we estimated separation indices for all phase function groups analysed here, averaging over the r_e values used in the CPP LUT (PS_r), but also over the v_e values examined for a given r_e (PS_v). This methodology, apart from providing a quantification for the explanation given before, and for similar argumentations given later, offers additional insights regarding angular ranges where retrievals should be expected to succeed or fail. Indeed, the PS_r index corresponding to Fig. 5c, which is plotted in supplementary Fig. S1, confirms that the main issues with retrieval failures should be expected near 133°, with secondarily problematic angles close to 141°, 177° and 180°, very similar to the findings of Cho et al. (2015).

3.2 Dependence of retrievals on the size distribution width

A similar analysis in the broader backscattering range (170°-180°) shows that the cause of the irregularities occurring in the cloud glory ~~is different~~can be more complicated. While phase function collapses can still occur, i~~I~~t is also known~~, in fact,~~

that the shape of the cloud glory depends on r_e and the width of the droplet size distribution, rather than τ. This has already been shown by ~~(see e.g.~~ Mayer et al., (2004) using reflectances at 753 nm and is also verified by our results. In fact, to verify the correct behavior of the CPP LUT in this respect, we examined the LUT reflectances under similar conditions but with thicker clouds (i.e. with multiple scattering prevailing). The southeastern Atlantic region and the MSG-1 observation geometry were selected, whereby both cloud bow and glory effects are apparent in the reflectances (Figs. 4c and 4e), during the same day (March 7, 2017). For each time slot, the viewing and illumination geometry and the r_e were those calculated from the spatial averages of the actual retrievals, while three values of τ were examined: $\tau = 1$ (very thin cloud), $\tau = 8$ (close to the average retrieved value) and $\tau = 30$ (thick cloud). Using the LUT with $v_e = 0.15$, we plotted the reflectances in the 0.6 µm channel corresponding to these cases. The results (Fig. S2) clearly show how an increased τ increases the reflectance measured by the satellite sensor. They also confirm that the cloud glory and cloud bow reflectance magnitudes relative to non-glory and non-bow time slots are not affected by τ. As Mayer et al. (2004) nicely described it: "The glory structure sits on top of a multiple-scattering background which of course depends on optical thickness".

Figure 6 shows how the phase function at 1.6 µm changes in the backscattering ~~range~~ intensity with varying r_e and v_e (phase functions at both 0.6 µm and 1.6 µm are shown for varying v_e). Figure 6a constitutes a zoom-in of Fig. 5c. It shows ~~that~~ how the angular distance of the characteristic cloud glory rings, appearing here as local maxima, from the 180° scattering angle, depends on the value of r_e for a given v_e. On the other hand, when r_e is given, the width of the size distribution controls the range of these maxima. This is depicted in both Figs. 6b and 6c for wavelengths $\lambda = 0.6$ µm and $\lambda = 1.6$ µm, respectively, and for a typical value of $r_e = 12$ µm and v_e ranging between 0.01 and 0.30. It is apparent in both plots that for narrow size distributions the cloud glory is enhanced.

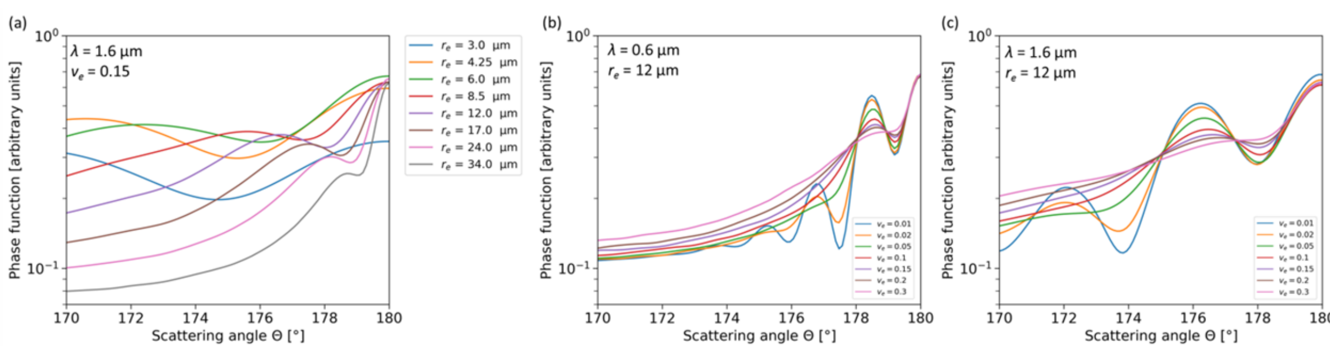

Figure 6: Dependence of the scattering phase function on r_e and v_e in the backscattering directions. (a) Phase functions at 1.6 µm wavelength used in the radiative transfer calculations for the eight r_e values of the LUTs, assuming $v_e = 0.15$. (b) Phase functions at 0~~1~~.6 µm wavelength used in the radiative transfer calculations for the seven v_e values of the LUTs, assuming $r_e = 12$ µm. (c) Same as in (b), but for phase functions at 1.6 µm.

Based on the previous analysis, it is natural to examine the CPP output under different assumptions regarding the width of the size distribution and the corresponding value of v_e. Figure 7 shows the differences between MSG-3 and MSG-1 τ and r_e retrievals for the seven v_e values examined. In the case of τ deviations occur only around the glory of each satellite, especially MSG-1, with the diurnal variation appearing smoother for narrower size distributions. These results show that the retrieval of τ is generally insensitive to the width of the size distribution, except for the cloud glory region. In the case of r_e ~~however~~, apart from the variation around the glory, large irregularities appear ~~in both the glory and~~also near the cloud bow regions (Fig 7b, see also Fig. 4f).~~, and their sensitivity to v_e is difficult to infer based on their differences (Fig. 7b). This is d~~ Due to the distance between the two satellites and the angular distance between cloud bow and glory, which are ~~similar,~~both close to 40°, the cloud glory from one satellite almost overlaps with the cloud bow from the other, rendering the assessment of the sensitivity to v_e difficult. Furthermore, as will be shown in Sect. 3.4, the assumption that retrievals from the two satellites are the same unless there is a cloud bow or glory condition does not always hold. Hence, the retrievals from the two satellites are re-examined separately, as shown in Fig. 8.

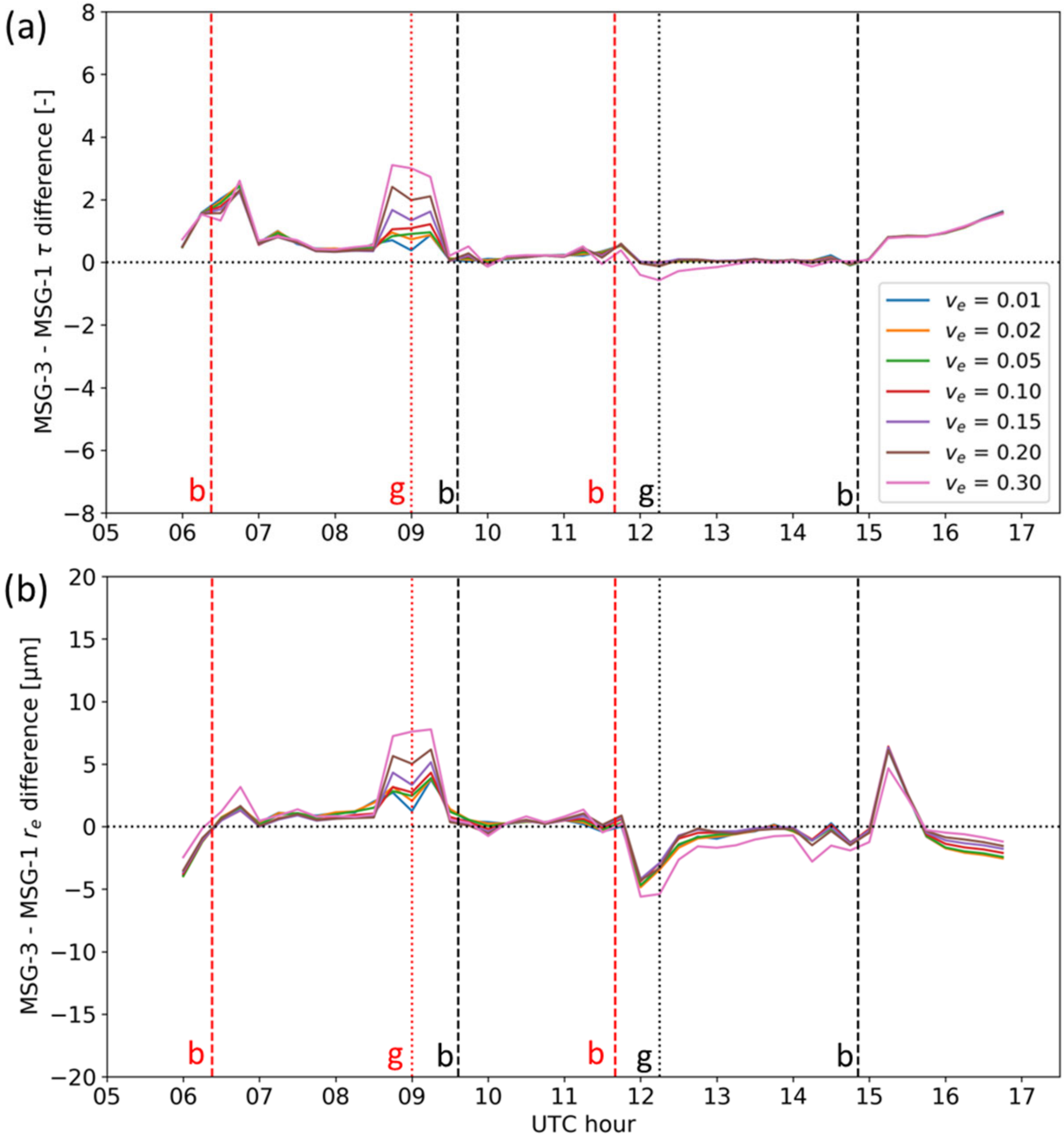

Figure 7: Differences between MSG-3 and MSG-1 retrievals of τ (a) and r_e (b) for the seven values of v_e examined, on March 7, 2017, over the southeastern Atlantic. The vertical lines represent cloud glory (dotted, denoted with “g”) and cloud bow (dashed, denoted with “b”) geometries for MSG-1 (red) and MSG-3 (black), as in Figure 2.

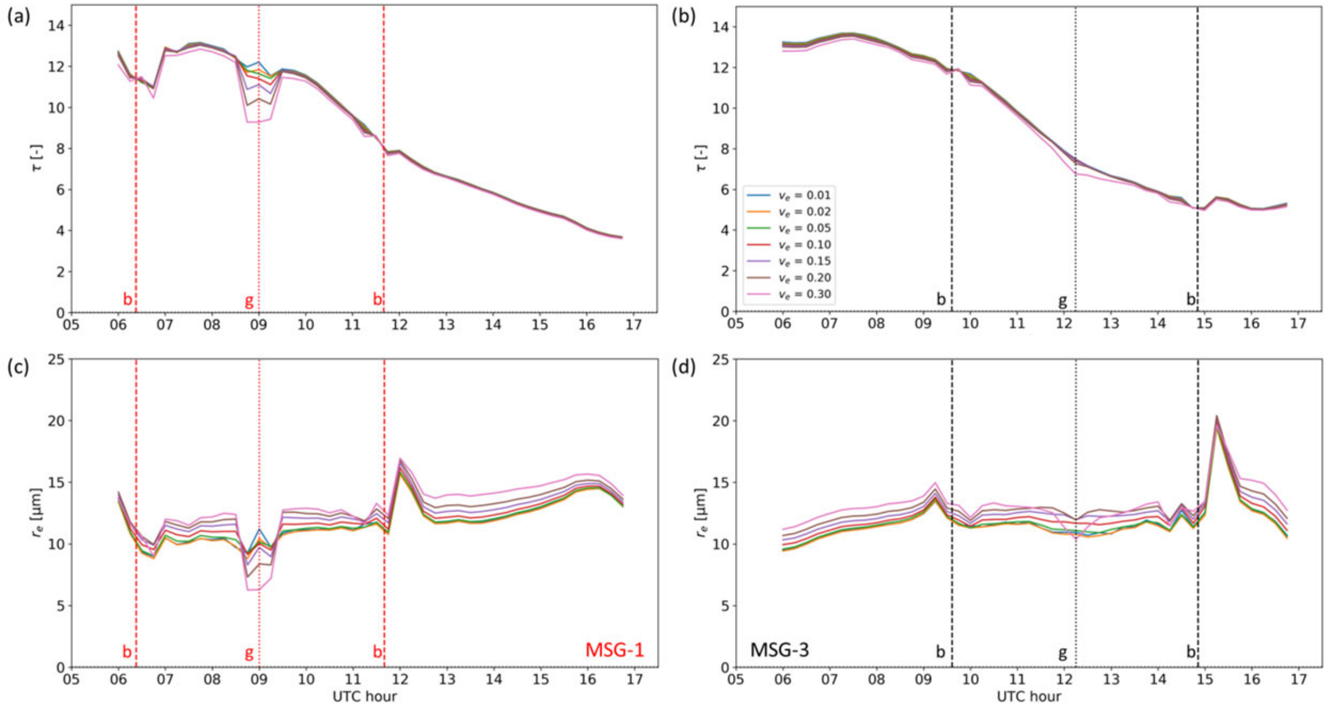

Figure 8: CPP retrievals of τ (a, b) and r_e (c, d) based on the 0.6 μm - 1.6 μm channel combination separately for MSG-1 (a, c) and MSG-3 (b, d), for the seven values of v_e examined, on March 7, 2017, over the southeastern Atlantic. The seven v_e values are shown in (b). The vertical lines represent cloud glory (dotted, denoted with "g") and cloud bow (dashed, denoted with "b") geometries for MSG-1 (red) and MSG-3 (black), as in Figure 2.

It is clear from Fig. 8 that v_e has a ~~significant~~ strong effect on r_e throughout the day, with differences occurring even during "normal" time slots. Based on the estimated τ and r_e uncertainties for the two extreme v_e values used, which control the spread of values in Fig. 8, it can be concluded that the difference between the τ retrievals for the extreme v_e values is smaller than the uncertainty, except in the glory of MSG-1, and the difference between the r_e retrievals for the extreme v_e values is larger than the uncertainty, except in the peak near the cloud bow. The effect of v_e on r_e in the glory is similar to that~~e~~ on τ ~~case~~under the same conditions, with larger irregularities for wider size distributions being apparent mainly in MSG-1. This difference between the two satellites should be attributed to the different maximum scattering angles: 176.4° for MSG-1 and 172.6° for MSG-3. An inspection of Fig. 6a, and especially the corresponding PS_r separation index (Fig. S3) shows that indeed MSG-1 would be more prone to failures (higher PS_r index values), and thus irregularities, than MSG-3. In the 133~~2~~° region~~, however,~~ there is no sensitivity to the size distribution width: all distributions deviate from adjacent time slots. This is because the phase function ~~overlapping~~collapse, shown in Fig. 5c, occurs for all values of v_e used.

Based on the irregularities near the cloud glory shown in Fig. 8 and the logical expectation that τ and r_e will exhibit a smooth diurnal variation, it appears that narrow droplet size distributions provide ~~more natural~~ outputs that are more consistent with this expectation. This is confirmed by examining the number of pixels which are flagged during the retrieval process, because the pair of VIS and SWIR reflectances lies outside the LUT. ~~Among others,~~ CPP provides these flags separately for pixels where the ~~pair of~~ reflectances lie~~s~~ ~~either~~ above or below the LUT. Figure 9 shows the percent number of these pixels in the study region separately for MSG-1 and MSG-3 and for flags above and below the LUT.

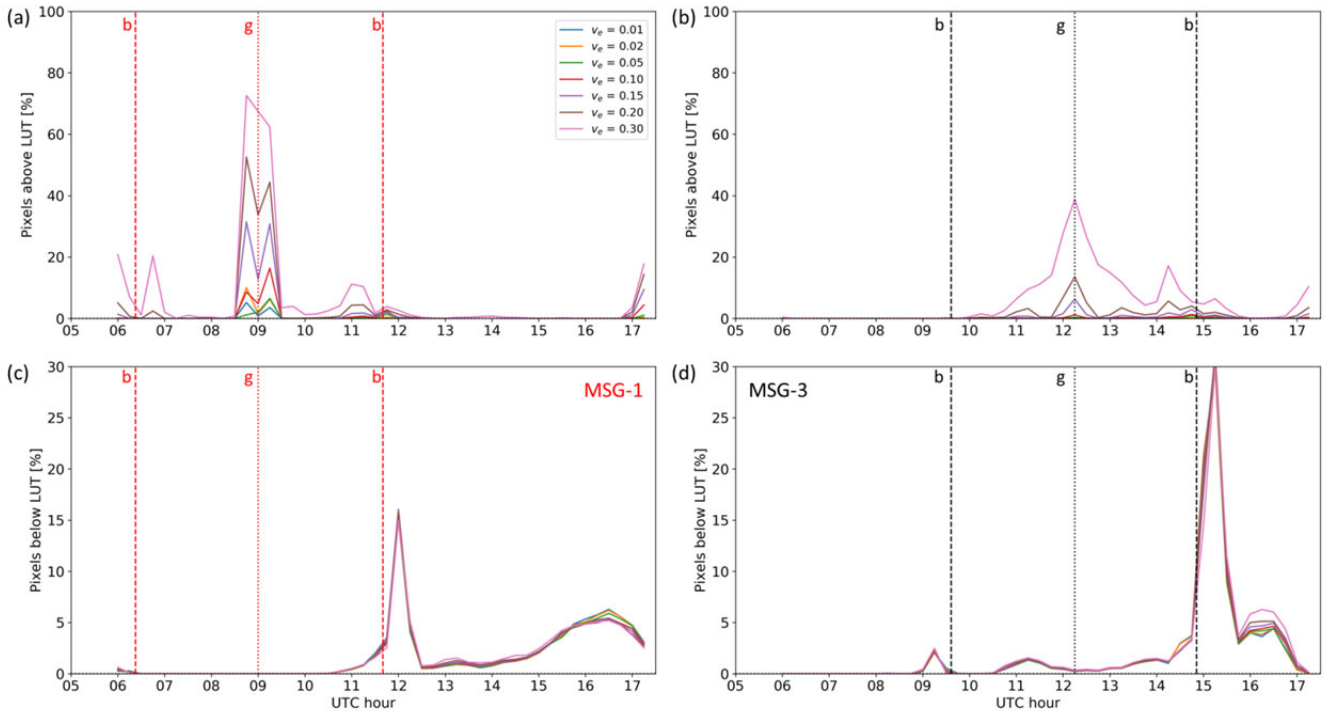

Figure 9: Fraction of flagged pixels (in %) with pairs of reflectances lying above (a, b) or below (c, d) the retrieval LUT, separately for MSG-1 (a, c) and MSG-3 (b, d) on March 7, 2017 over the southeastern Atlantic. The results are shown for seven LUTs, corresponding to the seven values of v_e shown in (a). The vertical lines represent cloud glory (dotted, denoted with "g") and cloud bow (dashed, denoted with "b") geometries for MSG-1 (red) and MSG-3 (black).

The number of flagged pixels above the LUT increases rapidly around the cloud glory for wide droplet size distributions, covering up to 4~~6~~0% and 7~~8~~0% of the study region when v_e is higher than 0.15, ~~. W~~while it appears that the narrower the size distribution, the ~~least~~ less retrieval failures~~, this does not necessarily mean that the actual droplet size distribution is so narrow~~. Distributions with larger widths will have relatively more small particles included (see Fig. 2a). For smaller particles the size parameter ($2\pi r/\lambda$) decreases, moving away from the regime where geometric optics hold, hence in these distributions ~~cannot capture~~ the cloud glory ~~adequately~~effect is much weaker, as can be seen in Figs. 6b and 6c. On the other hand, the "collapse" of the LUT which occurs around the cloud bow, due to the overlap of the phase functions, causes failures below the LUT, of the order of 20% (see also Fig. 5a). Secondary maxima in the flagged "above" pixels (Figs. 9a and 9b) occur for scattering angles slightly larger than 140° and are probably associated with the secondary peak in the PS_r index next to the cloud bow angles (Fig. S1). Note that, contrary to the failures associated with the primary peak of Fig. S1, depicted as pixels "below" in Figs. 9c and 9d, these failures occur above the LUT. Indeed, since the LUT collapses, the measurements may equally well lie above or below it. It should also be noted here that a comparison of Fig. 9 with Fig. S1 in terms of scattering angles where failures occur, highlights the difference between the failures near the cloud bow and those near the cloud glory: the former should be attributed to the collapse of the phase functions, whereas in the latter, where PS_r index values are much lower, selection of an appropriate v_e value plays the most important role.

3.3 Retrievals based on the 3.9 μm channel

CPP retrievals for the same day and region were repeated using the 0.6 μm - 3.9 μm channel combination, instead of the 0.6 μm - 1.6 μm. It is well known that retrievals at the former wavelength are more sensitive to the cloud top compared to the latter, at which the photons penetrate deeper into the cloud (Platnick, 2000). As a result, and because r_e varies vertically, corresponding retrievals are in principle different. Different failure patterns between the two spectral combinations have also been reported, with more successful retrievals for the larger wavelength, which is less prone to failures due to cloud inhomogeneity (Cho et al., 2015).

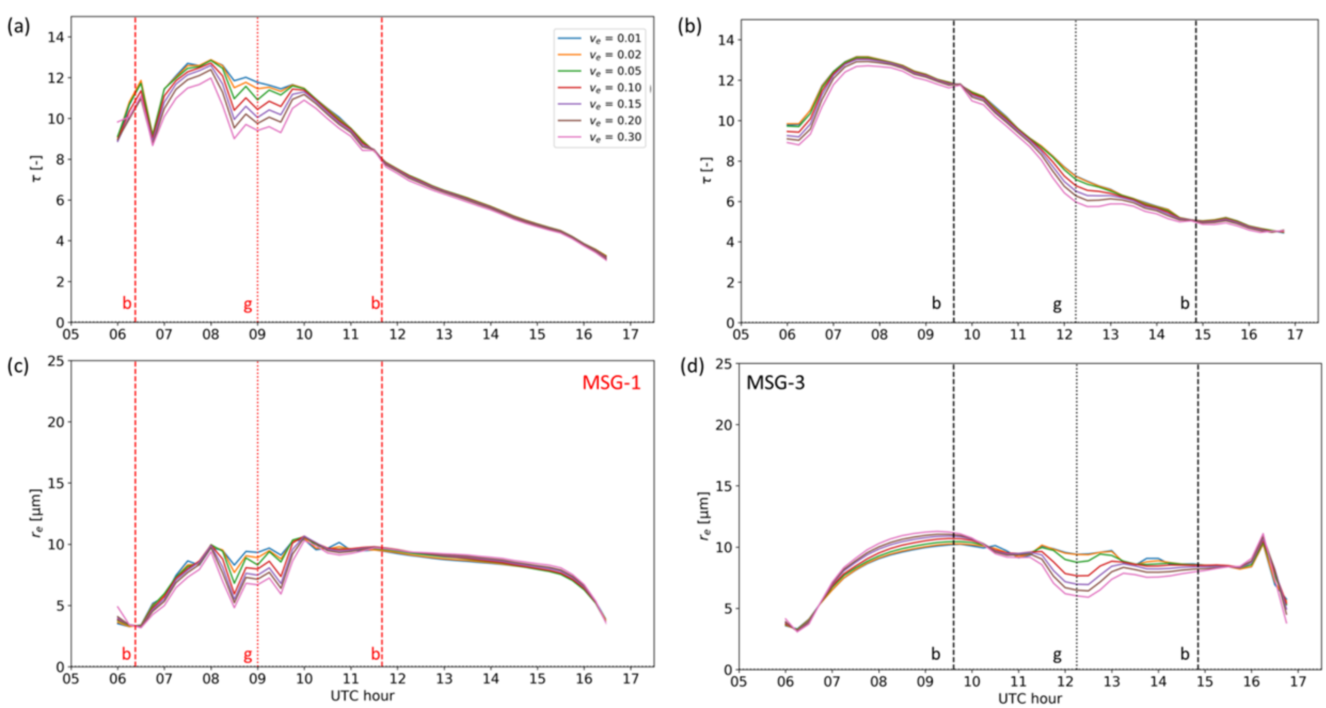

Figure 10: CPP retrievals of τ (a, b) and r_e (c, d) based on the 3.9 µm channel separately for MSG-1 (a, c) and MSG-3 (b, d), for the seven values of v_e examined, on March 7, 2017, over the southeastern Atlantic. The seven v_e values are shown in (a). The vertical lines represent cloud glory (dotted, denoted with "g") and cloud bow (dashed, denoted with "b") geometries for MSG-1 (red) and MSG-3 (black)~~, as in Figure 2~~.

Figure 10 shows the diurnal variation of τ and r_e retrieved using the 3.9 µm channel for the same day and region. Two prominent characteristics are directly distinguishable, compared to the corresponding 0.6 µm - 1.6 µm retrievals.~~: a)~~ First, a better discrimination of the diurnal patterns around the glory ~~corresponding to $v_e < 0.10$~~ is possible, especially in the case of MSG-3, which is as effective as MSG-1. In fact, in all panels of Fig. 10, the range of values in the glory and adjacent time slots is larger than the width of the uncertainty distributions.~~,~~ ~~and b)~~Second, there is no apparent irregularity near the cloud bow, which in the case of the 0.6 µm - 1.6 µm retrieval was caused by the phase functions overlap at 132° scattering angle. The first characteristic stems from the good separation level of phase functions in backscattering angles from both satellites, shown in Fig. 11a and verified by the corresponding PS_r index low values (Fig. S6). It also suggests that in this specific combination of spectral channels and viewing geometry additional information is available regarding the width of the size distribution. In fact, for scattering angles close to 172°, which is the angle in the glory time slot for MSG-3 in this specific day and region, the single scattering phase functions that correspond to different size distribution widths are much more separated at the 3.9 µm wavelength (Fig. 11b~~a~~) compared to the 1.6 µm (Fig. 6c~~b~~), as verified by the corresponding PS_v index values (Figs. S5 and S7). The low PS_v index values associated with this separation level (Fig. S7) hint further to a possibility of v_e retrieval under these specific conditions. The larger time range of retrievals sensitivity to r_e around the maximum scattering angle time slot compared to the 1.6 µm retrievals should be attributed to the glory features at 3.9 µm phase function which are also more widespread (Fig. 11a). The second characteristic originates in a similar feature, namely non-overlapping scattering phase functions of different r_e values in the 132° scattering angle region for the 3.9 µm wavelength (Fig. 11c~~b~~) compared to the ~~corresponding~~ overlapping phase functions for ~~the~~ 1.6 µm (Fig. 5c, see also corresponding PS_r index values in Fig. S8). This feature stems from the fact that for larger wavelengths the cloud bow, which is a geometrical optics phenomenon, is less pronounced, and renders the 3.9 µm channel more suitable for the retrieval of more realistic diurnal variations of cloud optical properties. Less retrieval failures compared to the 0.6 µm - 1.6 µm retrieval were also found, similarly to the results reported by Cho et al. (2015) on corresponding MODIS channels, although they never disappear completely from the cloud glory time slot. ~~They rather range between 20% and 60%, depending on satellite and v_e.~~ Near the cloud bow (132° scattering angle), however~~, (132° scattering angle)~~ they completely disappear.

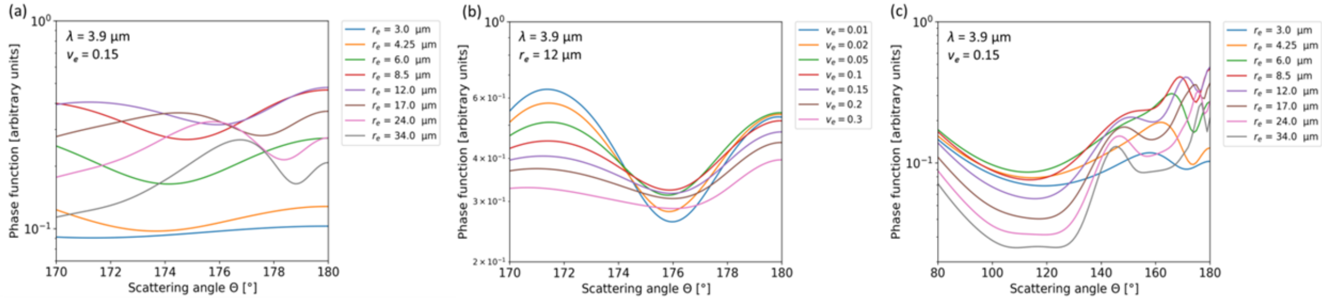

Figure 11: Dependence of the scattering phase functions at 3.9 µm wavelength on r_e and v_e ~~in the backscattering directions~~. (a) Phase functions in the backscattering directions for the ~~seven~~ eight r~~v~~$_e$ values of the LUTs,~~considered~~, assuming v~~r~~$_e$ = ~~12 µm~~0.15. (b) Phase functions for the ~~eight~~ seven v~~r~~$_e$ values ~~of the LUTs~~considered, assuming ~~r~~v$_e$ = ~~0.15~~12 µm. (c) As in (a), but for the scattering angle range 80° - 180°.

While a direct comparison of r_e values between the 0.6 µm - 1.6 µm and the 0.6 µm - 3.9 µm retrievals should be performed on a pixel basis, the overall smaller r_e values in the latter case hint to the presence of subpixel cloud heterogeneity (Zhang and Platnick, 2011). In fact, based on simulated MODIS retrievals, Bennartz and Rausch (2017) reported that for subpixel fractions of open water above 10% the retrieved r_e at 0.6 µm - 1.6 µm already starts to exceed the one retrieved at 0.6 µm - 3.9 µm. Apart from this, retrieval differences related to imperfect treatment of the 3.9 µm channel cannot be excluded, since this SEVIRI channel is rather broad and requires relatively large atmospheric correction.

3.4 Retrievals over the continental region

~~Part of t~~The results presented so far ~~are expected to~~ apply for specific circumstances, namely an optically ~~moderately thick~~thin marine Sc cloud over ocean. As previously explained, to examine possible differences caused by different cloud conditions, the same analysis was performed over a continental region, in the southern parts of Zimbabwe and Mozambique (19~~8~~°-21~~2~~° S, 30~~29~~°-32~~3~~° E, see also Fig. 1). The selection requirements here were also a spatial coverage of at least 80% with liquid clouds only, persistent in most time slots within a day. March 20, 2017 was selected, which is close to March 7, used in the marine case. Combined with the similar latitudes of the two regions, this ensures the presence of similar cloud glory and cloud bow conditions.

Retrievals based on the 0.6 µm - 1.6 µm channels for different values of v_e are shown in Figure 12. Values of τ reveal an optically much thicker cloud compared to the marine Sc case, with typical values between 20 and 30, increasing even further in late afternoon, while r_e values are also almost double those of the former case. ~~Lack of data in late afternoon is due to the liquid cloud fraction, which decreases below 80% in these time slots (see also Fig. 3b).~~ The cloud bow irregularities, especially in the r_e, are less pronounced compared to the marine region. ~~This should be attributed to the continental cloud being optically thicker, which leads to higher reflectance values. Hence, the~~This is due to the spectral pairs of cloudy pixels

~~will~~ lying~~ie~~ in the more orthogonal area of the LUT (see also Fig. 5), thus avoiding the LUT "collapse", which ~~will~~ affects thinner clouds. A closer look into the glory area, especially in the τ case, shows that larger v_e values now provide the smoother diurnal variability. This is consistent with thick continental clouds, for which wider size distributions are expected (Miles et al., 2000). It should be noted that, regarding τ, only in the glory time slots of MSG-3 are the uncertainty intervals for the retrievals at the extreme v_e values non-overlapping. In the case of r_e, only in "normal" time slots (neither cloud glory nor cloud bow) are the two extreme values well separated given their estimated uncertainties.

These results~~, however,~~ are not directly comparable with the marine Sc case: the ~~glory~~ maximum scattering angles here ~~occurs at~~are 177°-178°~~ scattering angle~~ for both satellites. Compared to the 172° and even the 176° of MSG-3 and MSG-1 in the marine case, respectively, scattering phase function characteristics at the 0.6 µm channel (~~not~~ shown in Fig. 6b), where τ retrieval is sensitive, can already differ significantly (see also the corresponding PS_v index in Fig. S4). A similar argument holds for r_e retrieval and corresponding angle and phase function differences in the 1.6 µm channel (Figs. 6c~~b~~ and S5). It should also be noted that, contrary to the marine case, retrievals between the two satellites differ rather substantially in both absolute values and diurnal variability. While 3D effects from the specific cloud type could be causing these differences, the latter were not further investigated, since they do not compromise our results: effects of using different v_e values are still apparent in the individual satellite retrievals.

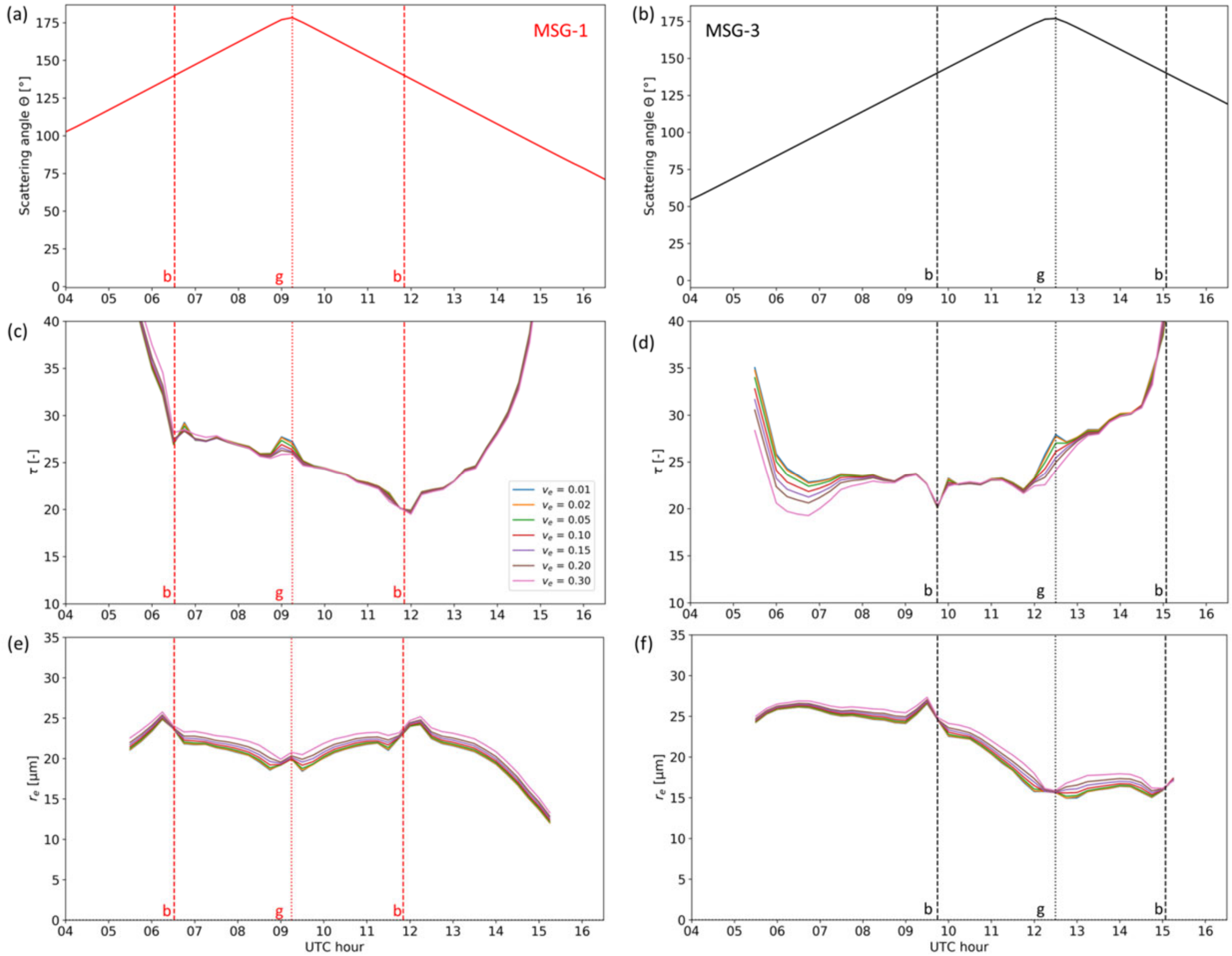

Figure 12: Scattering angles (a, b) and CPP retrievals of τ (c~~a~~, d~~b~~) and r_e (e~~c~~, f~~d~~) based on the 0.6 µm - 1.6 µm channel separately for MSG-1 (~~a, c~~left column) and MSG-3 (~~b, d~~right column), for the seven values of v_e examined, on March 20, 2017, over the continental region shown in Fig. 1. The vertical lines represent cloud glory (dotted, denoted with “g”) and cloud bow (dashed, denoted with “b”) geometries for MSG-1 (red) and MSG-3 (black)~~, as in Fig. 2~~.

Figure 13 shows corresponding CPP output over the continental region using the 0.6 µm - 3.9 µm channels. As was also implied from the 0.6 µm - 1.6 µm retrievals over the same region (Fig. 12), wider distributions with v_e around 0.15 appear more realistic, with uncertainties in v_e = 0.01 and v_e = 0.30 non-overlapping in the τ retrievals around the MSG-3 glory. The value of v_e also appears to affect the r_e retrieval throughout the day: higher v_e lead to higher r_e values, except near the glory region, where this pattern is reversed. For “non-glory” time slots, the range of r_e values found is also larger than the uncertainties. The absence of any cloud bow feature, and the collapse of r_e retrievals near the cloud glory can again be attributed to corresponding 3.9 μm phase function characteristics in these scattering angles (see also Figs. 11c~~b~~ and 11b~~a~~ respectively).

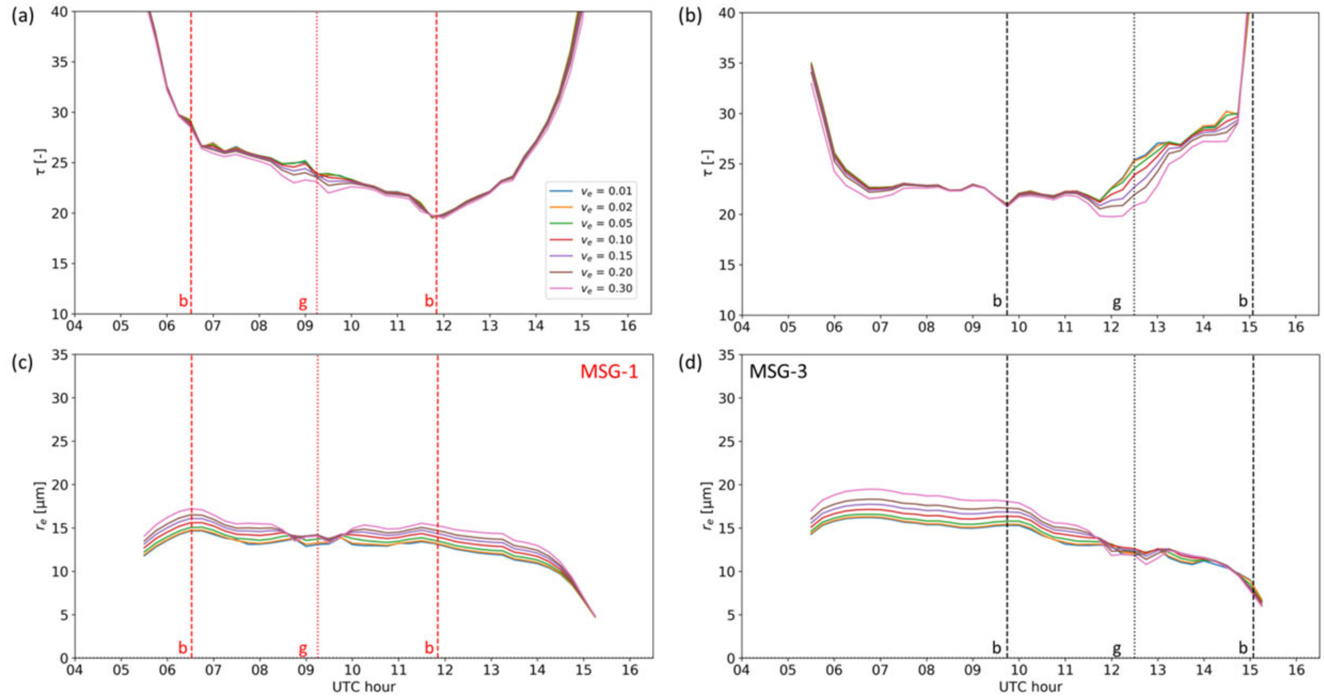

Figure 13: CPP retrievals of τ (a, b) and r_e (c, d) based on the 3.9 μm channel separately for MSG-1 (a, c) and MSG-3 (b, d), for the seven values of v_e examined, on March 20, 2017, over the continental region shown in Fig. 1. The vertical lines represent cloud glory (dotted, denoted with “g”) and cloud bow (dashed, denoted with “b”) geometries for MSG-1 (red) and MSG-3 (black)~~, as in Fig. 2~~.

Regarding failure rates in the continental case, it is important noting that in the glory time slot they generally lie ~~around~~ below 10%, never exceeding 20% in any channel combination and v_e value, while in the cloud bow they lie around 20% in the 0.6 μm - 1.6 μm retrieval and practically disappear in the 0.6 μm - 3.9 μm, similarly to the marine case. Since the maximum backscattering angles are quite different between the marine and the continental case, decreased numbers of flagged pixels in the latter case might be due to this difference.

4 Discussion and Summary

In the present study irregularities in retrieved τ and r_e from satellite-based passive imagers were investigated using two MSG satellites. The importance of these irregularities is corroborated by the frequency of their occurrence: based on the way scattering angles change during a day, cloud bow irregularities will manifest twice per day in any region. Irregularities associated with cloud glory, on the other hand, require high values of scattering angles. Due to the position of both satellites along the equator, these conditions are met in days close to the two equinoxes. Taking advantage of the large overlap area between MSG-1 and MSG-3, a marine and a continental region were analyzed under different illumination and viewing conditions. While in principle the common retrieval algorithm should compensate for the different viewing and illumination geometries, and the two satellite products over the same region should agree under any circumstances, monitoring the diurnal evolution of the retrieved optical properties revealed that this is not the case. Results showed that ~~these~~ irregularities in this diurnal evolution are related to scattering phase function characteristics near the cloud bow and cloud glory domains. In the latter case, retrievals were found to be sensitive to the width of the assumed droplet size distribution, expressed by v_e. Retrievals based on different SWIR wavelengths also showed that the smaller wavelength (1.6 μm) is more sensitive to cloud bow-induced irregularities than the larger (3.9 μm).

The analysis conducted here raises the question of the most appropriate value of v_e assumed in the retrieval. Measurements from many campaigns have been used for the estimation of the width of the droplet size distribution (see e.g. tables 1 and 2 in Miles et al., 2000 and table 1 in Igel and Van den Heever, 2017). If the corresponding width measures reported in these studies are converted to v_e, they lead to a range of values very similar to 0.01-0.30, as was used in Arduini et al. (2005) and in the present study. These results are not contradictory, since different size distribution widths are expected for different cloud types and under different conditions.

Table 2. Typical values and ranges of v_e found in observational studies and corresponding review papers.

Cloud type	v_e (±1σ)
Continental (Miles et al., 2000)	0.20 ± 0.17
Marine (Miles et al., 2000)	0.17 ± 0.15
Marine Sc (Miles et al., 2000)	0.13 ± 0.08
Marine Sc (Mayer et al., 2004)	0.01 ± 0.002
Marine Sc (Painemal & Zuidema, 2011)	0.07 ± 0.04 (average profile)
	0.04 ± 0.04 (cloud top)
Shallow Cu (Igel & van den Heever, 2017)	0.09 ± 0.04

Table 2 summarizes ~~-~~ v_e values obtained from existing observational studies, where different measures of the width of the droplet size distribution were converted to v_e. The v_e values from Miles et al. (2000) and Igel & van den Heever (2017) were based on their tables, in which results from various measurement campaigns are summarized. The continental and marine average values from Miles et al. (2000) are based on all values from their tables 2 and 1, respectively, while the marine Sc average from the same study is calculated based only on the clouds denoted "Sc" in their table 1. Wider droplet size distributions are generally found in continental clouds compared to marine ones. ~~In m~~Marine ~~only clouds,~~ Sc decks exhibit even narrower distributions. A very narrow size distribution, corresponding to v_e = 0.01, was deduced from Mayer et al. (2004) based on aircraft measurement specifically in the cloud glory area, where information on the distribution width is available. Additionally, Painemal and Zuidema (2011), presenting results from a measurement campaign over the Southeast Pacific Sc deck, report values of the "*k*" parameter, which is an equivalent measure of the size distribution width, varying with cloud height. Specifically, they estimate values of k equal to 0.8 and 0.88 for the average profile and the cloud-top respectively, which correspond to v_e equal to 0.07 and 0.04. ~~More recently~~Lately, Grosvenor et al. (2018) provided a useful discussion on the effect of the size distribution width on the estimation of CDNC and concluded that a value of 0.10 for v_e is likely to be an overestimation. More recently, Di Noia et al. (2019) attempted retrieving v_e based on a neural network approach and observations from POLDER-3. Their results show a tendency of the algorithm to also retrieve narrow distributions over ocean ($v_e \sim 0.05$).

The conclusions drawn from the present study are similar, showing that the assumption of narrower distributions, with v_e around 0.05, leads to more reasonable retrievals, at least for the marine Sc cloud type. ~~This is further emphasized by~~Instead, ~~the results over the continental region (Sect. 3.4), where~~ a wider size distribution appears more reasonable over the continental region (Sect. 3.4). These differences suggest that, in future retrievals, a cloud type- or region-specific v_e selection prior to retrieval would probably lead to more realistic results under cloud glory conditions.~~,~~ Viewed from the opposite direction, and along with the additional information provided by using different spectral pairs (Sect. 3.3), the results of this study highlight the potential of passive geostationary imagers to retrieve v_e under specific circumstances. The required information seems to be available in the cloud glory time slot, and a retrieval attempt could be based on an "irregularities minimization" scheme applied to the diurnal variability of the retrieved τ and r_e. Alternatively, apart from the τ and r_e dimensions in the LUT, an additional v_e dimension could be added, in time slots when corresponding phase functions appear well separated (i.e. near cloud glory conditions). ~~and~~ Plans for the next CM SAF CLAAS and CLARA cloud data records include updating the v_e used to a lower value, based on the present results.~~future research will focus on the attempt to retrieve v_e from SEVIRI in regions with homogeneous liquid cloud cover under glory illumination conditions.~~

Author contributions

N.B. and J.F.M. developed the methodology. J.F.M. performed the retrievals. N.B. performed the analysis. All authors contributed in interpreting the results, writing, editing and finalizing the manuscript.

Competing interests

The authors declare that they have no conflict of interest.

Acknowledgements

This work was performed within CM SAF funded by EUMETSAT.

References

Arduini, R. F., Minnis, P., Smith, W. L., Ayers, J. K., Khaiyer, K. K., and Heck, P.: Sensitivity of satellite-retrieved cloud properties to the effective variance of cloud droplet size distribution, Proc. 15th ARM Science Team Meeting, 2005.

Benas, N., Finkensieper, S., Stengel, M., van Zadelhoff, G.-J., Hanschmann, T., Hollmann, R., and Meirink, J. F.: The MSG-SEVIRI-based cloud property data record CLAAS-2, Earth Syst. Sci. Data, 9, 415-434, doi: 10.5194/essd-9-415-2017, 2017.

Bennartz, R. and Rausch, J.: Global and regional estimates of warm cloud droplet number concentration based on 13 years of AQUA-MODIS observations, Atmos. Chem. Phys., 17, 9815-9836, doi: 10.5194/acp-17-9815-2017, 2017.

Cho, H. M., Zhang, Z., Meyer, K., Lebsock, M., Platnick, S., Ackerman, A. S., Di Girolamo, L., Labonnote, L., Cornet, C., Riedi, J., and Holz, R.: Frequency and causes of failed MODIS cloud property retrievals for liquid phase clouds over global oceans, J. Geophys. Res.- Atmos., 120, 4132-4154, doi: 10.1002/2015JD023161, 2015.

CM SAF: Algorithm Theoretical Basis Document, SEVIRI Cloud Physical Products, CLAAS Edition 2, EUMET SAT Satellite Application Facility on Climate Monitoring, SAF/CM/KNMI/ATBD/SEVIRI/CPP, Issue 2, Rev. 2, doi: 10.5676/EUM_SAF_CM/CLAAS/V002, 2016a.

CM SAF: Algorithm Theoretical Basis Document, CM SAF Cloud, Albedo, Radiation data record, AVHRR-based, Edition 2 (CLARA-A2), Cloud Physical Products, EUMETSAT Satellite Application Facility on Climate Monitoring, SAF/CM/SMHI/ATBD/CPP_AHVRR issue 2.0, 19/08/2016, doi: 10.5676/EUM_SAF_CM/CLARA_AVHRR/V002, 2016b.

De Haan, J. F., Bosma, P., and Hovenier, J. W.: The adding method for multiple scattering calculations of polarized light, Astron. Astrophys., 183, 371–391, 1987.

De Rooij, W. A. and Van der Stap, C. C. A. H.: Expansion of Mie scattering matrices in generalized spherical functions, Astron. Astr., 131, 237–248, 1984.

Derrien, M. and Le Gléau, H.: MSG/SEVIRI cloud mask and type from SAFNWC, Int. J. Remote Sens., 26, 4707–4732, 2005.

Di Noia, A., Hasekamp, O. P., van Diedenhoven, B., and Zhang, Z.: Retrieval of liquid water cloud properties from POLDER-3 measurements using a neural network ensemble approach, Atmos. Meas. Tech., 12, 1697-1716, doi: 10.5194/amt-12-1697-2019, 2019.

Greuell, W., Meirink, J. F., and Wang, P.: Retrieval and validation of global, direct, and diffuse irradiance derived from SEVIRI satellite observations, J. Geophys. Res., 118, 2340–2361, doi:10.1002/jgrd.5019, 2013.

Grosvenor, D. P., Sourdeval, O., Zuidema, P., Ackerman, A., Alexandrov, M. D., Bennartz, R., et al.: Remote sensing of droplet number concentration in warm clouds: A review of the current state of knowledge and perspectives, Rev. Geophys., 56. doi: 10.1029/2017RG000593, 2018.

Hansen, J.: Multiple scattering of polarized light in planetary atmospheres. Part II. Sunlight reflected by terrestrial water clouds, J. Atmos. Sci., 28, 1400–1426, 1971.

Heidinger, A. K., Foster, M. J., Walther, A., and Zhao, Z.: The Pathfinder Atmospheres Extended (PATMOS-x) AVHRR climate data set, B. Am. Meteorol. Soc., 95, 909–922, doi: 10.1175/BAMS-D-12-00246.1, 2014.

Igel, A. L., and S. C. van den Heever: The importance of the shape of cloud droplet size distributions in shallow cumulus clouds. Part I: Bin microphysics simulations, J. Atmos. Sci., 74, 249–258, doi: 10.1175/JAS-D-15-0382.1, 2017.

Karlsson, K.-G., Riihelä, A., Müller, R., Meirink, J. F., Sedlar, J., Stengel, M., Lockhoff, M., Trentmann, J., Kaspar, F., Hollmann, R., and Wolters, E.: CLARA-A1: a cloud, albedo, and radiation dataset from 28 yr of global AVHRR data, Atmos. Chem. Phys., 13, 5351–5367, doi:10.5194/acp-13-5351-2013, 2013.

Karlsson, K.-G., Anttila, K., Trentmann, J., Stengel, M., Meirink, J. F., Devasthale, A., Hanschmann, T., Kothe, S., Jääskeläinen, E., Sedlar, J., Benas, N., van Zadelhoff, G.-J., Schlundt, C., Stein, D., Finkensieper, S., Håkansson, N., and Hollmann, R.: CLARA-A2: the second edition of the CM SAF cloud and radiation data record from 34 years of global AVHRR data, Atmos. Chem. Phys., 17, 5809-5828, doi: 10.5194/acp-17-5809-2017, 2017.

Können, G. P.: Rainbows, halos, coronas and glories. Beautiful sources of information, Bull. Amer. Meteor. Soc., 98, 485–494, doi: 10.1175/BAMS-D-16-0014.1, 2017.

Liang, L., Di Girolamo, L., and Sun, W.: Bias in MODIS cloud drop effective radius for oceanic water clouds as deduced from optical thickness variability across scattering angles, J. Geophys. Res.-Atmos., 120, 7661–7681, doi: 10.1002/2015JD023256, 2015.

Mayer, B., Schröder, M., Preusker, R., and Schüller, L.: Remote sensing of water cloud droplet size distributions using the backscatter glory: a case study, Atmos. Chem. Phys., 4, 1255-1263, doi: 10.5194/acp-4-1255-2004, 2004.

McGarragh, G. R., Poulsen, C. A., Thomas, G. E., Povey, A. C., Sus, O., Stapelberg, S., Schlundt, C., Proud, S., Christensen, M. W., Stengel, M., Hollmann, R., and Grainger, R. G.: The Community Cloud retrieval for CLimate (CC4CL) – Part 2: The optimal estimation approach, Atmos. Meas. Tech., 11, 3397-3431, doi: 10.5194/amt-11-3397-2018, 2018.

Meirink, J. F., Roebeling, R. A., and Stammes, P.: Inter-calibration of polar imager solar channels using SEVIRI, Atmos. Meas. Tech., 6, 2495-2508, doi: 10.5194/amt-6-2495-2013, 2013.

Miles, N. L., J. Verlinde, and E. E. Clothiaux: Cloud droplet size distributions in low-level stratiform clouds, J. Atmos. Sci., 57, 295–311, 2000.

Nakajima, T. and King, M. D.: Determination of the Optical Thickness and Effective Particle Radius of Clouds from Reflected Solar Radiation Measurements, Part 1: Theory, J. Atmos. Sci., 47, 1878–1893, 1990.

NWC SAF: Algorithm Theoretical Basis Document for the Cloud Product Processors of the NWC GEO, EUMETSAT Satellite Application Facility on Nowcasting and Short range Forecasting, NWC/CDOP2/GEO/MFL/SCI/ATBD/Cloud, Issue 1, Rev. 1, 15 October 2016.

Painemal, D. and Zuidema, P.: Assessment of MODIS cloud effective radius and optical thickness retrievals over the Southeast Pacific with VOCALS-REx in situ measurements, J. Geophys. Res., 116, D24206, doi: 10.1029/2011jd016155, 2011.

Pavolonis, M. J., Heidinger, A. K., and Uttal, T.: Daytime global cloud typing from AVHRR and VIIRS: Algorithm description, validation, and comparison, J. Appl. Meteorol., 44, 804–826, doi: 10.1175/JAM2236.1, 2005.

Petty, G. W. and Huang, W.: The modified gamma size distribution applied to inhomogeneous and nonspherical particles: Key relationships and conversions, J. Atmos. Sci., 68, 1460–1473, doi: 10.1175/2011JAS3645.1, 2011.

Pincus, R., Platnick, S., Ackerman, S. A., Hemler, R. S., and Hofmann, R. J.: Reconciling simulated and observed views of clouds: MODIS, ISCCP, and the limits of instrument simulators, J. Clim., 25, 4699-4720, doi: 10.1175/JCLI-D-11-00267.1, 2012.

Platnick, S.: Vertical photon transport in cloud remote sensing problems, J. Geophys. Res., 105, 22 919–22 935, doi: 10.1029/2000JD900333, 2000.

Platnick, S., Meyer, K. G., King, M. D., Wind, G., Amarasinghe, N., Marchant, B., Arnold, G. T., Zhang, Z., Hubanks, P. A., Holz, R. E., Yang, P., Ridgway, W. L., and Riedi, J.: The MODIS cloud optical and microphysical products: Collection 6 updates and examples from Terra and Aqua, IEEE Trans. Geosci. Remote Sens., 55, 502–525, doi: 10.1109/TGRS.2016.2610522, 2017.

Roebeling, R. A., Feijt, A. J., and Stammes, P.: Cloud property retrievals for climate monitoring: implications of differences between SEVIRI on METEOSAT-8 and AVHRR on NOAA-17, J. Geophys. Res., 111, D20210, doi: 10.1029/2005JD006990, 2006.

Rossow, W. B.: Climate Data Record Program (CDRP): Climate Algorithm Theoretical Basis Document (C-ATBD) International Satellite Cloud Climatology Project (ISCCP) H-Series, CDRPATBD-0872, Asheville, North Carolina, USA, 179 pp., 2017.

Seemann, S.W., E. E. Borbas, R. O. Knuteson, G. R. Stephenson, H.-L. Huang: Development of a Global Infrared Land Surface Emissivity Database for Application to Clear Sky Sounding Retrievals from Multi-spectral Satellite Radiance Measurements, J. Appl. Meteorol. Clim., 47, 108-123, 2008.

Seethala, C., Meirink, J. F., Horváth, Á., Bennartz, R., and Roebeling, R.: Evaluating the diurnal cycle of South Atlantic stratocumulus clouds as observed by MSG SEVIRI, Atmos. Chem. Phys., 18, 13283-13304, doi: 10.5194/acp-18-13283-2018, 2018.

Stammes, P.: Spectral radiance modelling in the UV-Visible range, IRS 2000: Current problems in Atmospheric Radiation, edited by: Smith, W. L. and Timofeyev, Y. M., A. Deepak Publ., Hampton, VA, 385–388, 2001.

Stengel, M., Kniffka, A., Meirink, J. F., Lockhoff, M., Tan, J., and Hollmann, R.: CLAAS: the CM SAF cloud property data set using SEVIRI, Atmos. Chem. Phys., 14, 4297-4311, doi: 10.5194/acp-14-4297-2014, 2014.

Stengel, M., Stapelberg, S., Sus, O., Schlundt, C., Poulsen, C., Thomas, G., Christensen, M., Carbajal Henken, C., Preusker, R., Fischer, J., Devasthale, A., Willén, U., Karlsson, K.-G., McGarragh, G. R., Proud, S., Povey, A. C., Grainger, R. G., Meirink, J. F., Feofilov, A., Bennartz, R., Bojanowski, J. S., and Hollmann, R.: Cloud property datasets retrieved from AVHRR, MODIS, AATSR and MERIS in the framework of the Cloud_cci project, Earth Syst. Sci. Data, 9, 881-904, doi: 10.5194/essd-9-881-2017, 2017.

Walther, A. and Heidinger, A. K.: Implementation of the Daytime Cloud Optical and Microphysical Properties Algorithm (DCOMP) in PATMOS-x, J. Appl. Meteorol. Clim., 51, 1371–1390, doi:10.1175/JAMC-D-11-0108.1, 2012.

Wood, R.: Stratocumulus clouds, Mon. Weather Rev., 140, 2373– 2423, doi: 10.1175/MWR-D-11-00121.1, 2012.

Wood, R. and Hartmann, D. L.: Spatial Variability of Liquid Water Path in Marine Low Cloud: The Importance of Mesoscale Cellular Convection, J. Clim., 19, 1748–1764, 2006.

Young, A. H., Knapp, K. R., Inamdar, A., Hankins, W., and Rossow, W. B.: The International Satellite Cloud Climatology Project H-Series climate data record product, Earth Syst. Sci. Data, 10, 583-593, doi: 10.5194/essd-10-583-2018, 2018.

Zeng, S., Cornet, C., Parol, F., Riedi, J., and Thieuleux, F.: A better understanding of cloud optical thickness derived from the passive sensors MODIS/AQUA and POLDER/PARASOL in the A-Train constellation, Atmos. Chem. Phys., 12, 11245-11259, doi: 10.5194/acp-12-11245-2012, 2012.

Zhang, Z. and Platnick, S.: An assessment of differences between cloud effective particle radius retrievals for marine water clouds from three MODIS spectral bands, J. Geophys. Res.-Atmos., 116, D20215, doi:10.1029/2011JD016216, 2011.

Zhou, C., Zelinka, M. D., and Klein, S. A.: Impact of decadal cloud variations on the Earth's energy budget Nat. Geosci., 9, 871–874, doi: 10.1038/ngeo2828, 2016.